Plant Cell Advance Publication. Published on August 2, 2018, doi:10.1105/tpc.18.00426

RESEARCH ARTICLE

Predominant Golgi Residency of the Plant K/HDEL Receptor Is Essential for its Function in Mediating ER Retention

Fernanda A.L. Silva-Alvim[1], Jing An[1], Jonas C. Alvim[1], Ombretta Foresti[1,2], Alexandra Grippa[1], Alexandra Pelgrom[1], Thomas L. Adams[1], Chris Hawes[3], and Jurgen Denecke[*,1]

[1] Centre for Plant Sciences, School of Biology, Faculty of Biological Sciences, University of Leeds, Leeds LS2 9JT, United Kingdom.
[2] Current address: Cell and Developmental Biology Programme, Center for Genomic Regulation, Universitat Pompeu Fabra, Barcelona, Spain.
[3] Department of Biological and Medical Sciences, Faculty of Health and Life Sciences, Oxford Brookes University, Gipsy Lane, Headington, Oxford, OX3 0AZ, UK.
*Corresponding author: j.denecke@leeds.ac.uk

Short title: Retention in the endoplasmic reticulum

One-sentence summary: A novel functional fluorescent protein fusion of the K/HDEL-receptor ERD2 reveals that its Golgi residency is crucial for biological function and depends on a conserved di-leucine motif.

The author responsible for distribution of materials integral to the findings presented in this article in accordance with the policy described in the Instructions for Authors (www.plantcell.org) is: Jurgen Denecke (j.denecke@leeds.ac.uk).

ABSTRACT

Accumulation of soluble proteins in the endoplasmic reticulum (ER) of plants is mediated by a receptor termed ER RETENTION DEFECTIVE 2 (ERD2) or K/HDEL receptor. Using two gain-of-function assays and by complementing loss of function in *Nicotiana benthamiana* we discovered that compromising the lumenal N-terminus or the cytosolic C-terminus with fluorescent fusions abolishes its biological function and profoundly affects its subcellular localization. Based on the confirmed asymmetrical topology of ERD2 we engineered a new fluorescent ERD2 fusion protein that retains biological activity. Using this fusion, we show that ERD2 is exclusively detected at the Golgi apparatus, unlike non-functional C-terminal fusions which also label the ER. Moreover, ERD2 is confined to early Golgi compartments and does not show ligand-induced redistribution to the ER. We show that the cytosolic C-terminus of ERD2 plays a crucial role in its function. Two conserved Leucine residues that do not correspond to any known targeting motifs for ER-Golgi trafficking were shown to be essential for both ERD2 Golgi residency and its ability to mediate ER retention of soluble ligands. The results suggest that anterograde ER to Golgi transport of ERD2 is either extremely fast, well in excess of the bulk flow rate, or that ERD2 does not recycle in the way originally proposed.

INTRODUCTION

Since the discovery of the vectorial nature of the secretory pathway linking the endoplasmic reticulum (ER) via the Golgi apparatus to the plasma membrane (Palade, 1975), it has become clear that it is one of the most ancient innovations of the emerging eukaryotes. The discovery

that soluble proteins secrete by default (Wieland et al., 1987) and require signals for cell retention, either in the ER (Munro and Pelham, 1987) or the vacuole (Valls et al., 1987) was a turning point in our understanding of the secretory pathway. Post-Golgi protein sorting has evolved slightly differently in plants, yeasts and fungi (Dacks et al., 2008; Klinger et al., 2016). By contrast, the ER retention of soluble proteins displaying C-terminal tetrapeptides KDEL or HDEL appears to be remarkably conserved (Denecke et al., 1992).

The receptor that sorts KDEL or HDEL proteins was identified via an elegant genetic screen in *Saccharomyces cerevisiae* and is encoded by the *ER retention defective 2* (*ERD2*) gene (Semenza et al., 1990). ERD2 homologs were subsequently found in other eukaryotes, including plants (Lee et al., 1993). In mammalian cells ERD2 is mostly localized to the Golgi apparatus (Lewis and Pelham, 1990; Griffiths et al., 1994; Tang et al., 1993) from where it specifically retrieves soluble ER proteins for recycling back to the ER (Pelham, 1988; Lewis et al., 1990). Although extensive mutagenesis experiments revealed amino acids that were important in either ligand-binding or receptor transport (Townsley et al., 1993; Scheel and Pelham, 1998), the signals controlling ERD2 transport between the ER and the Golgi, as well as mechanisms that prevent post Golgi trafficking of ERD2 remain elusive (Pfeffer, 2007).

The predicted 7 transmembrane domain structure (Townsley et al., 1993) is reminiscent of the G-protein-coupled-receptor (GPCR) family (Capitani and Sallese, 2009), further supported by a shift in its steady state distribution to the ER upon ligand binding (Lewis and Pelham, 1992). However, overexpressed ERD2 alone was shown to mediate a Brefeldin A (BFA)-like effect (Hsu et al., 1992) and redistributed to the ER, alongside other secretory cargo, in the absence of overproduced ligands. It has been shown that ERD2 also recruits ARF1-GAP to Golgi membranes (Aoe et al., 1997), a process that could be exacerbated by KDEL-binding to the receptor (Majoul et al., 2001). An alternative model suggests that a cascade of interactions exist between ligands, ERD2, G-proteins and protein kinase A (Cabrera et al., 2003; Pulvirenti et al., 2008; Cancino et al., 2014). How either of these models explains the transport of K/HDEL proteins back to the ER is unclear.

The difficulty associated with studying ERD2 function lies in the fact that anterograde and retrograde transport between the ER and the Golgi strictly depend on each other (Brandizzi and Barlowe, 2013), and complete ERD2 knockout is lethal (Townsley et al., 1994; Mei et al., 2017). Mutants of one of the *ERD2* genes in *Arabidopsis thaliana* exhibited low expression levels of one of three calreticulin gene products (Li et al., 2009) but had no effect on other ER

resident HDEL proteins. Functional studies on ERD2 were based on *in vitro* peptide binding assays which were not verified by *in vivo* complementation assays monitoring the transport of soluble ligands (Townsley et al., 1993; Scheel and Pelham, 1998; Cabrera et al., 2003). Moreover, the proposed 7-transmembrane domain structure was challenged by two independent reports using either N-linked glycosylation probes (Singh et al., 1993) or redox-sensitive GFP fusions to N- and C-termini of ERD2 (Brach et al., 2009), both proposing an even number of transmembrane domains. Therefore, it appears that one of the most conserved steps in the secretory pathway is one of the least understood processes and justifies a new approach towards understanding its mechanism.

To directly monitor the function of ERD2 *in vivo* and to establish sorting principles that control receptor localization, we introduce two bio-assays based on a strong gain-of-function effect of ectopic ERD2 expression *in vivo*. We can either monitor the dose-responsive inhibition of soluble cargo secretion biochemically, or visualize the ER retention *in situ* using an engineered fluorescent Golgi membrane marker harbouring a C-terminal HDEL. We show that *ERD2* genes from *Arabidopsis thaliana* and *Nicotiana benthamiana* increase the capacity for ER retention. An antisense-inhibition and complementation assay shows that ERD2 can be functionally interchanged between these two plant species. Using these tools we show that direct N-terminal or C-terminal fluorescent ERD2 fusions used in previous studies (Boevink et al., 1998; Li et al., 2009; Xu and Liu, 2012; Xu et al., 2012; Montesinos et al., 2014) are non-functional. A re-evaluation of the ERD2 topology established a lumenal N-terminus and a cytosolic C-terminus. By introducing an additional transmembrane domain at the N-terminus of ERD2, we succeeded in generating a biologically active fluorescent ERD2 fusion that preserves the functional core of ERD2. Interestingly, this active fusion protein is predominantly Golgi-resident, irrespective of ligand dosage. Using this fusion we could demonstrate a previously unrecognized crucial role of the cytosolic tail of ERD2 in promoting both Golgi residency and biological function. The findings form an important platform from which further work can be explored, towards a better understanding of one of the first protein sorting steps in the secretory pathway.

RESULTS

A quantitative gain-of-function assay for the *ERD2* gene product

Barley α-amylase (Amy) has been successfully used as a cargo molecule in numerous studies as it can be quantified by a robust enzymatic assay, is readily secreted and can be re-directed to the ER or the vacuole via fusion to sorting signals (Phillipson et al., 2001; Foresti et al., 2010). The Amy C-terminus adequately exposed tetrapeptides such as HDEL or KDEL to the sorting machinery and led to an approximately 10-fold reduced secretion in *Nicotiana tabacum* protoplasts (Figure 1A). Two longer fusions harboring the last 34 amino acids of the calreticulin C-terminus, either with (Amy-CRT2) or without the HDEL motif (Amy-CRT2ΔHDEL) demonstrated that the acidic C-domain of calreticulin could increase cell retention further (Amy-CRT2, Figure 1C). However, it was unlikely a consequence of a better HDEL display because the acidic C-terminus alone without the HDEL motif reduced secretion as well (Figure 1A, compare first and last lane). A signal-independent retention mechanism (Rose and Doms, 1988; Sönnichsen et al., 1994) was suggested to be mediated by calcium-chelating properties and/or association with endogenous ER residents rather than interactions with ERD2 (Koch, 1987; Macer and Koch, 1988; Rose and Doms, 1988). We thus used Amy-HDEL and Amy-KDEL as cargo molecules to study ERD2 function as these fusions rely solely on their tetrapeptide signals to be retained in the cells and ideally suitable as ERD2 model cargo.

As partial ER retention of HDEL proteins (Phillipson et al., 2001) is likely to be caused by saturation of endogenous ERD2 which mimics a partial ERD2 loss-of-function phenotype, we wanted to test if additional ERD2 proteins can specifically suppress HDEL-saturation and resultant secretion, which would provide a gain-of-function assay for ERD2. Therefore, the *Arabidopsis thaliana ERD2a* coding region (Lee et al., 1993) was inserted into a dual expression vector (DV) similar to those introduced earlier (Bottanelli et al., 2011) but harbouring the Golgi-marker ST-CFP instead of ST-YFP (Sparkes et al., 2006; Brandizzi et al., 2002). The Golgi-marker served as a transfection control in immunoblots and to check the integrity of the Golgi apparatus in situ (Figure 1D, Effector plasmid).

Transfection *of Nicotiana benthamiana* Amy-HDEL plasmid consistently revealed a higher initial secretion index compared to *Nicotiana tabacum* protoplasts (Figure 1E). Co-transfection with increasing amounts of DV vector with ERD2a effector strongly reduced the partial secretion of Amy-HDEL in a dose-dependent manner (Figure 1E). A control experiment using secreted Amy as non-ligand cargo revealed no significant effect of ERD2a on constitutive secretion. Protein levels of the transfection control ST-CFP were comparable for the Amy and Amy-HDEL co-expression experiments, and Golgi morphology was punctate with no evidence

for ER structures (Figure 1F). This shows that the level of ectopic ERD2a expression was well below the threshold above which ERD2-induced BFA-like effects on the ER-Golgi system have been reported (Hsu et al., 1992). A further control experiment in which ERD2a was replaced by the cytosolic enzyme phosphinotricine acetyl transferase (PAT, Bottanelli et al., 2011) showed that the internal Golgi-marker ST-CFP had no effect on amy-HDEL transport (Figure 1G). Together the data show that we have developed a highly sensitive ERD2 gain-of-function assay that is specific to HDEL-proteins and permits quantitative dose-response assays.

Plant ERD2 isoforms are functionally conserved

The tetrapeptides KDEL and HDEL both prevent reporter protein secretion equally well in plant cells (Denecke et al., 1992; Pimpl et al., 2006) but it is unknown if this is due to different receptors with different affinities. *Arabidopsis thaliana* contains two related *ERD2* genes with the same overall number of amino acids and 68% sequence identity. The second gene, here called *ERD2b*, was proposed to be a specific receptor for *Arabidopsis thaliana* calreticulin 3 (CRT3) but not other ER residents harbouring HDEL signals (Li et al., 2009). We repeated the gain-of-function assay in *Nicotiana tabacum* protoplasts with the two *Arabidopsis thaliana* ERD2 isoforms (ERD2a and ERD2b) and showed that they display the same dose-responses for Amy-HDEL (Figure 2A) as well as Amy-KDEL as cargo molecule (Figure 2B). The two signals as well as the two receptors were fully interchangeable, and the specific effect of the mutant *ERD2b* allele on CRT3 only (Li et al., 2009) may reflect properties of CRT3 rather than ERD2. The result also shows that the dose-response assay works in two different *Nicotiana* species, even though absolute secretion indexes are different. All further experiments were carried out with *Nicotiana benthamiana* protoplasts because its available genome sequence permits gene knock-down experiments.

As in Arabidopsis and all land plants, *Nicotiana benthamiana* contains two *ERD2* genes, which are closely related to their Arabidopsis counterparts exhibiting 80 and 83% sequence identity. To engineer an *ERD2* knockdown in *Nicotiana benthamiana* with a single construct, we created a hybrid *ERD2* transcript (*NbERD2ab*) and generated sense and anti-sense overexpression constructs (Figure 2C). Figure 2D shows that sense expression of the engineered hybrid *NbERD2ab* conveyed increased amy-HDEL retention comparable to that of *Arabidopsis thaliana ERD2b*. Expression of the anti-sense construct (AS) resulted in elevated levels of amy-HDEL secretion, consistent with a partial *ERD2* knock-down. Since Arabidopsis

ERD2b shows significant sequence divergence at the nucleotide level compared to the *Nicotiana benthamiana* hybrid, its transcript was expected to be resistant to the effects of the anti-sense inhibition. Indeed, co-expression of sense *Arabidopsis thaliana ERD2b* abolished the effect of *NbERD2ab* anti-sense expression and mediated strong retention of Amy-HDEL.
The results indicate that both ERD2 isoforms in two plant species can be considered functionally equivalent, and the complementation of the partial gene knock-down confirms the gain of function assay (Figure 1) which allows quantitative monitoring of ERD2 function. Since *Arabidopsis thaliana* ERD2a and ERD2b were fully interchangeable, all further experiments to elucidate ERD2 function in plants were carried out with Arabidopsis ERD2b which is generally higher expressed compared to ERD2a (Schmid et al., 2005), hereafter simply referred to as ERD2.

ERD2-mediated ER retention *in situ*

To visualise ERD2-mediated cargo accumulation in the ER *in situ*, it was necessary to establish a model that permits detection of fluorescence in the ER and in a post-ER compartment with high sensitivity. We took advantage of the fact that HDEL-mediated ER retention has been reported for the SNARE Sec20 (Sweet and Pelham, 1992), a type II membrane spanning protein with a lumenal C-terminus. We thus used the Golgi marker ST-YFP (Brandizzi et al., 2002) as it is also a type II membrane protein with YFP exposed in the lumen of the secretory pathway. To test if this molecule can serve as cargo for ERD2, the tetrapeptide HDEL was fused to the C-terminus of ST-YFP (Figure 3A) in order to create a fluorescent cargo molecule (ST-YFP-HDEL) that can be studied *in situ*.
The coding regions for ST-YFP and ST-YFP-HDEL were placed under the transcriptional control of the weak *TR2* promoter (Bottanelli et al., 2012) to avoid overexpression-induced labelling of ST-YFP in transit through the ER (Boevink et al., 1998) and possible leakage to post-Golgi compartments. Agrobacterium-mediated transient expression in infiltrated tobacco leaf epidermis cells followed by confocal laser scanning microscopy analyses revealed that under these conditions, ST-YFP was efficiently transported from the ER to the Golgi bodies and therefore undetectable in transit through the ER (Figure 2B, first panel). However, addition of the HDEL tetrapeptide to the lumenal C-terminus caused a total retention of the fusion protein in the ER (Figure 3B, second panel), suggesting that HDEL-mediated ER retention

takes precedence over potential ER export and Golgi localization signals of this Golgi membrane marker.

To cause HDEL-saturation, secreted amylase (Amy) or ER-retained Amy-HDEL was over-expressed using the strong CaMV35S promoter construct placed on the same *Agrobacterium* vector T-DNA harboring ST-YFP-HDEL. Whilst Amy had no effect on ST-YFP-HDEL, co-expressed Amy-HDEL caused a partial re-distribution of the reporter back to the typical punctate structures of Golgi bodies (Figure 3B, compare third and fourth panel). The Golgi membrane marker does not progress beyond the Golgi apparatus and accumulates to high concentrations (Boevink et al., 1998; Brandizzi et al., 2002), thus providing a very sensitive saturation assay.

To carry out an ERD2 gain-of-function assay *in situ*, a second *Agrobacterium* strain harbouring a dual expression T-DNA encoding ST-RFP as independent Golgi marker together with either a mock effector (PAT) or ERD2 was used. Figure 3C shows that punctate ST-YFP-HDEL structures induced by Amy-HDEL were indeed Golgi bodies as they co-localized with ST-RFP when co-expressed with the mock effector PAT. Correlation analysis via the Pearson-Spearman correlation (PSC) plug-in for ImageJ (French et al., 2008) which quantifies red and green fluorescence from individual pixels showed a high positive correlation (Rs above + 0.5) when punctate structures (white arrow heads) were analyzed. However, in the presence of ERD2, the ST-RFP punctae lost the co-localization with ST-YFP-HDEL which was fully ER retained again (Figure 3D). Punctate structures were now almost exclusively red fluorescent (white arrow heads), and RFP and YFP fluorescence showed no correlation (Rs below 0), in spite of occasional areas with close apposition of ER and Golgi structures. Supplemental Figure 1 shows the merged images of Figure 3C and D in alternative colors, where co-localization at the level of the Golgi is reflected by a white-shifted blue or magenta color of the punctate structures.

Together, the results so far illustrate that we can quantify ERD2 function biochemically by measuring increased cell retention of a soluble cargo (Figures 1&2), and *in situ* by showing the increased fluorescence of an HDEL-harbouring membrane cargo when it is redistributed from the Golgi to the ER network (Figure 3).

N- and C-terminal fluorescent tagging abolishes ERD2 activity and influences subcellular localization

C-terminal fluorescent ERD2 fusion proteins including ERD2-GFP, ERD2-CFP and ERD2-YFP have been repeatedly used in the literature to reveal a dual ER-Golgi localization (Boevink et al., 1998; daSilva et al., 2004; Xu and Liu, 2012; Montesinos et al., 2014). To test if C-terminal fluorescent ERD2 fusions are biologically active, we inserted the coding region for untagged ERD2 as well as ERD2-YFP into the GUS reference vector (Figure 4A) to routinely quantify and equalize transfection efficiency more accurately than by protein gel blots (Gershlick et al., 2014). We first established experimental conditions to obtain comparable GUS levels, and then used those conditions to compare different ERD2 constructs. Figure 4B (upper panel) shows that in sharp contrast to untagged ERD2, ERD2-YFP did not reduce secretion of Amy-HDEL, despite comparable transfection as documented by the GUS control (Figure 4B, lower panel). It is possible that the proposed signalling function for the ERD2 C-terminus (Cabrera et al., 2003; Pulvirenti et al., 2008; Cancino et al., 2014) is masked by the fluorescent protein, rendering the receptor inactive.

We next generated an N-terminal YFP fusion with ERD2 (YFP-ERD2). Analysis using the same GUS-reference plasmid also failed to document biological activity in Amy-HDEL retention (Figure 4B). Interestingly, subcellular localization of ERD2-YFP and YFP-ERD2 revealed two very different patterns. ERD2-YFP was well expressed and labelled the ER and the Golgi apparatus (Figure 4C) whilst YFP-ERD2 was difficult to detect and trapped in the ER (Figure 4D). The localization result for ERD2-YFP is in agreement with earlier studies using similar C-terminal ERD2 fusions but contradict a study showing that such a fusion can reduce secretion of HDEL proteins (Montesinos et al., 2014).

Very low expression and ER retention of YFP-ERD2 may be indicative of severe misfolding, perhaps by flipping the orientation of ERD2 in the membrane. We thus introduced an N-terminal signal peptide and a short decapeptide harbouring an N-linked glycosylation site (Batoko et al., 2000) to the N-terminus of YFP-ERD2. Figure 4B shows that the resulting construct (secYFP-ERD2) still failed to show any biological activity. However, in sharp contrast to YFP-ERD2, secYFP-ERD2 labelled exclusively punctate structures (Figure 4E) and was now well expressed. Co-expression with the Golgi-marker ST-RFP confirmed that the structures are indeed Golgi bodies (Supplemental Figure 2A). When co-expressed with the ERD2-cargo RFP-HDEL, no co-localization was detected (Supplemental Figure 2B).

Finally, we re-created an internal fusion protein which places YFP within the first predicted cytosolic loop of ERD2 (Supplemental Figure 3A). This fusion was originally reported as being

Golgi-localized (Li et al., 2009), but its ability to increase the retention of HDEL cargo was not tested. Surprisingly, this fusion protein (E-YFP-RD2) was completely undetectable in Agrobacterium-infiltrated leaves. The discrepancy may be caused by the fact that the original fusion protein was driven by the *Arabidopsis thaliana ERD2b* promotor and included intron sequences which were omitted here to provide fair comparisons with other constructs shown in Figure 4. Multi-copy expression using the GUS-reference plasmid under the control of the CaMV35S promoter in protoplasts at the highest plasmid concentration revealed weak diffuse cytosolic fluorescence in between chloroplasts and other organelles in less than 1% of the protoplasts. This is well below the usual 10% transfection efficiency and suggests that the protein is very poorly expressed, despite very high levels of the internal reference marker GUS (Supplemental Figure 3B). The Amy-HDEL transport assay revealed no biological activity, suggesting that this protein is non-functional as well.

In conclusion, all published fluorescent ERD2 fusions as well as a newly introduced fusion (secYFP-ERD2) are non-functional in the Amy-HDEL assay, and show a variety of subcellular localizations, ranging from weak cytoplasmic (E-YFP-RD2), weak ER (YFP-ERD2), strong ER-Golgi (ERD2-YFP) and very strong Golgi (secYFP-ERD2) localization.

A lumenal N-terminus is important for Golgi-localization of ERD2

The most dramatic difference was observed between ER-retained YFP-ERD2 and the Golgi resident secYFP-ERD2. Since signal peptides are cleaved, only a flipped membrane topology can explain such a different fate of the fusion protein. To investigate this further, we first tagged the new secYFP-ERD2 construct with RFP at its C-terminus. The resulting construct secYFP-ERD2-RFP was well expressed and showed a dual ER-Golgi localization in both channels (Figure 4F), similar to ERD2-YFP (Figure 4C). This shows that the secYFP portion does not cause dominant Golgi retention and that C-terminal tagging promotes partial ER localization of ERD2-fusions. The YFP portion was shown to be glycosylated (Figure 4G) as observed by a size shift of the full-length fusion protein fusion induced by the N-linked glycosylation inhibitor tunicamycin (T), suggesting that the YFP portion is lumenal. A similar dual expression construct without an N-terminal signal peptide (YFP-ERD2-RFP) was very poorly expressed and only weakly detected in the ER (data not shown), similar to YFP-ERD2 (Figure 4D). By contrast, secYFP-ERD2 protein levels are high, it readily leaves the ER and accumulates in the

Golgi, which suggests that it is correctly folded. We concluded that a lumenal N-terminus is essential to mediate ER export and high expression of ERD2 at the Golgi apparatus.

A fluorescently tagged ERD2 that retains biological activity

To understand ERD2 function, it is important to trace the subcellular localization of functional ERD2 *in vivo*. To preserve a functional core of ERD2 and avoid obstructing either terminus or obstructing internal regions, we tested if extending ERD2 by an additional transmembrane domain could place the fluorescent tag out of harm's way. To minimize the chance to upset the transmembrane structure of ERD2, we took advantage of the existence of an *ERD2*-related gene family termed ERPs (Hadlington and Denecke, 2000) which is uniquely found in plants as well as Stramenopiles, Alveolates and Rhizaria collectively termed the SAR-group (Klinger et al., 2016) but absent in other eukaryotes including the Excavata, Amoebozoa, yeasts/fungi and animals. Figure 5A shows a comparison between ERP1 (AT4G38790) and ERD2b, illustrating the overall similarity with the ERD2 core, but with an additional N-terminal domain harbouring an additional transmembrane domain. The possibility that ERPs and ERD2 either evolved from a common ancestor or evolved from each other justifies the rationale of our approach. We thus fused YFP to the N-terminus of ERP1 and also created fluorescent hybrids between ERP1 and ERD2, by inserting the additional TM domain to the N-terminus or the C-terminus prior to fusion to YFP and RFP (Figure 5B).

YFP-ERP1 was well expressed even under control of the weak *TR2* promoter and was localized to the ER (Figure 5C, first row). YFP-TM-ERD2 was Golgi localized and could not be detected in the ER (Figure 5C, second row). ERD2-TM-RFP was localized to both the ER and the Golgi apparatus (Figure 5C, third row), similar to ERD2-YFP (Figure 4C) and secYFP-ERD2-RFP (Figure 4F). When these constructs were analyzed via the gain-of-function assay using the GUS reference vector to test biological activity, C-terminally tagged ERD2-TM-RFP was non-functional (Figure 5D) and essentially behaved like ERD2-YFP (Figure 4B, C). By contrast, N-terminally tagged YFP-TM-ERD2 showed clear albeit reduced ability to promote increased amy-HDEL retention (Figure 5D). Replacing the YFP portion by RFP (RFP-TM-ERD2) also yielded a biologically active fusion protein with activity similar to that of YFP-TM-ERD2. A further construct containing the additional TM alone (TM-ERD2) showed similar biological activity compared to the native ERD2 (Figure 5D, last two lanes). We also tested the ability of YFP-TM-ERD2 to complement the partial gene knock-down by the antisense

NbERD2ab hybrid (AS). Figure 5E shows that the fusion protein could abolish the effect of the antisense at low dose and mediate further amy-HDEL retention at higher dose.

The combined results show that N-terminal tagging of ERD2 can result in Golgi-localized fluorescent fusions as long as the ERD2 N-terminus is lumenal, either by forcing YFP into the lumen with a signal peptide (secYFP-ERD2, Figure 4E,G) or by using cytosolic YFP followed by an additional transmembrane domain. However, only the latter retains biological activity, suggesting that the lumenal side of the ERD2 N-terminus must remain un-obstructed. In addition, the ERD2 C-terminus must remain unaltered.

ERD2 has a cytosolic C-terminus

Having established a lumenal N-terminus, we studied the C-terminus by comparing a direct fusion at the C-terminus (ERD2-RFP) with ERD2-TM-RFP, both of which show the same dual Golgi-ER localization (Figure 5C, data not shown). A proteinase K protection experiment on total microsomes expressing ERD2-RFP revealed a resistant RFP core fragment in the presence or absence of detergent (Figure 6A). However, ERD2-TM-RFP revealed a specific protected polypeptide fragment (PF) of a higher molecular weight compared to RFP-core (Figure 6A, black arrowhead). The molecular weight of the PF was consistent with the presence of a single TM fused to RFP and it was degraded in the presence of detergent, unlike the resistant RFP-core which provided a loading control. This indicates that ERD2-TM-RFP produces a fusion protein with a lumenal RFP due to the additional TM domain.

To verify that N-termini and C-termini do not influence each other, we supplemented ERD2-TM-RFP with secYFP at its N-terminus, yielding secYFP-ERD2-TM-RFP that can be detected with two different antibodies. The resulting larger polypeptide continues to be glycosylated, as seen by the size shift of the full-length polypeptide in the presence of tunicamycin (Figure 6A). The same size shift was seen in Figure 4F, showing that the YFP portion at the N-terminus is lumenal regardless of the insertion of an additional C-terminal TM. Furthermore, protease protection of secYFP-ERD2-TM-RFP microsomes revealed the same protected RFP fragment (black arrow heads) as seen for ERD2-TM-RFP. This shows that presence of secYFP to the N-terminus did not change the membrane orientation of the ERD2 C-terminus either.

When probed with antibodies to YFP, the full-length secYFP-ERD2-TM-RFP fusion protein (FL) also exhibited a tunicamycin-sensitive size shift (Figure 6B). Protease protection revealed a PF corresponding to glycosylated YFP fused to the complete ERD2 polypeptide but without

the fused additional TM and RFP (black arrowheads). The results suggest that all the predicted cytosolic loops of ERD2 are resistant to the protease, except for the artificially created loop at the C-terminus by adding a further TM domain. Again in the presence of detergent the PF was digested, leaving only the proteinase K resistant YFP-core which served as a loading control.
Based on these results, together with the results of Figures 4 and 5, we propose that native ERD2 possesses an asymmetrical membrane topology with a lumenal N-terminus and a cytosolic C-terminus. The resulting topology of the experimental constructs is illustrated in Figure 6C.

ERD2 resides mainly at the cis-Golgi apparatus

In situ activity and subcellular localization of the new fluorescent fusion proteins was tested by our *in situ* assay (Figure 3B). RFP-TM-ERD2 labelled exclusively punctate structures when co-expressed with ST-YFP-HDEL together with either Amy (Figure 7A) or Amy-HDEL (Figure 7B). Even in the presence of the competitor Amy-HDEL, ST-YFP-HDEL always showed complete retention in the ER network, with no detectable punctate structures (see Supplemental Figure 4 for alternative color schemes). This demonstrates that RFP-TM-ERD2 increases the ER retention capacity and confirms the results from the biochemical bio-assays (Figure 5D) *in situ*.
The exclusively punctate labelling of RFP-TM-ERD2 was also observed for YFP-TM-ERD2 and the two fusions co-localized to a high level (Figure 7C). Co-expression of the standard Golgi marker ST-YFP with RFP-TM-ERD2 also revealed co-localization in the same structures (Figure 7D), as seen for the combination YFP-TM-ERD2 with ST-RFP (Figure 5C). A thorough analysis of many images revealed that although RFP-TM-ERD2 labelled the same structures as ST-YFP, a stratification of the structures into predominantly red (open arrow head) or predominantly green (white arrow head) structures resulted in a slightly lower correlation coefficient and a broader distribution in the scatterplots (Figure 7D).
A stratified fluorescence could be reminiscent of cis-trans segregation. To characterize the new ERD2 fusion further, we included YFP-SYP61 as a *trans*-Golgi network (TGN) marker in the analysis (Dettmer et al., 2006). RFP-TM-ERD2 did not label YFP-SYP61 structures when co-expressed, resulting in a negative correlation coefficient and distinct green-only and red-only populations in scatterplots (Figure 7E). Occasionally, the two types of organelle could be observed in close vicinity to each other leading to partial overlap in fluorescent signals (white stars) but these were transient encounters. Similar results were obtained when comparing

YFP-SYP61 with the Golgi marker ST-RFP (Foresti and Denecke, 2008), showing completely different organelles in plants.

To enhance the resolution at the level of the Golgi stack, we used the Airyscan function in conjunction with a higher magnification and a narrower pinhole to assess co-localization and potential segregation between the Golgi marker ST-RFP and YFP-TM-ERD2. Under these experimental conditions, it became obvious that YFP-TM-ERD2 continued to co-localize well with RFP-TM-ERD2 (Figure 8A), as seen by a main diagonal yellow population in the scatter plot and a high positive correlation coefficient (+0.76). By contrast, co-expression of ST-RFP with YFP-TM-ERD2 clearly revealed structures labelled by ST-RFP only (Figure 8B, white arrowheads), represented by a distinct red-only population in the scatter plot. This resulted in a much lower correlation coefficient (+0.46) than observed with conventional confocal laser scanning microscopy (+0.69, Figure 7B). All structures labelled by YFP-TM-ERD2 were also labelled with ST-RFP, showing that the ERD2 fusion perhaps does not proceed as far in the Golgi stack as the trans Golgi marker ST-RFP.

We also co-expressed the functional RFP-TM-ERD2 with the earlier constructed non-functional secYFP-ERD2 for analysis using the Airyscan detector (Figure 8C). The very high degree of co-localization shows that secYFP-ERD2 may not exhibit any protein sorting defects. However, the function of secYFP-ERD2 is completely abolished, possibly due to interference by the lumenal YFP which could block ligand-binding.

Together, the results show that the new biologically functional fluorescent ERD2 fusions are mainly localized to the cis-cisternae of the Golgi bodies, from which ERD2-mediated recycling of HDEL proteins is thought to occur (Phillipson et al., 2001). The Golgi-marker ST-RFP is found in the same structures but can also proceed to the trans-cisternae (Boevink et al., 1998; Ito et al., 2012).

ERD2 Golgi-residence is ligand-independent

Interestingly, YFP-TM-ERD2 and RFP-TM-ERD2 did not reveal any ER–localization, even in the presence of ligands ST-YFP-HDEL and Amy-HDEL (Figure 7B). This is in contrast to earlier work documenting redistribution of ERD2 upon co-expression of KDEL ligands in transfected mammalian cells (Lewis and Pelham, 1992) and plants (Montesinos et al., 2014). To increase the potential for ligand-saturation, we switched back to the protoplast model as it permits multi-copy gene-expression and thus higher HDEL levels in individual cells. Since

ERD2 overexpression alone could cause its redistribution to the ER (Hsu et al., 1992), we wanted to achieve higher levels of HDEL cargo compared to the experiments in Figure 1, but at the same time avoid ERD2 overexpression. Therefore, we constructed new triple expression vectors to harbour 1) the *GUS* gene for normalisation of transfection, 2) the cargo molecule Amy (either with or without HDEL) under control of the strong CaMV35S promoter and 3) the biologically active fusion protein YFP-TM-ERD2 under control of the extremely weak promoter pNOS (enjoy the map in Supplemental Methods 2).

Transient expression experiments were normalized with the reporter GUS and designed to reach saturating expression levels of Amy-HDEL in the presence of the fluorescent ERD2 fusion. Figure 8D shows that under these conditions the distribution of YFP-TM-ERD2 remains exclusively Golgi localized, either in the presence of the non-ligand Amy or the ligand Amy-HDEL. Maximum intensity projections failed to visualize any hint of the ER network when Amy-HDEL was co-expressed (Figure 8E). Measurement of the secretion index in the corresponding protoplast suspensions confirmed that Amy-HDEL secretion was not affected by co-expressed YFP-TM-ERD2 from the same plasmid, compared to expression of Amy-HDEL alone, demonstrating that ligands were present well in excess of added receptor fusions due to the choice of promoters. In addition, expression from a single plasmid vector ensures that individual cells with the highest YFP fluorescence signals will also have highest Amy-HDEL levels. Together with data in Figure 7 A,B, the data show that ligand-induced re-distribution of ERD2 as observed for mammalian cells (Lewis and Pelham, 1992) could not be observed in plants under any of the experimental conditions tested.

Interestingly, tubular extensions from ERD2-labelled Golgi bodies could be seen with YFP-TM-ERD2 (Figure 8B) as well as secYFP-ERD2 (Figure 4E). These tubular emanations from Golgi bodies were not ER tubules, as they were only shown to co-localize with ST-YFP (Figure 8B), not with the ER-retained ST-YFP-HDEL (Figure 7A, B). Tubules were observed to connect two or more adjacent Golgi bodies (Supplemental Movie 1) which appear to tether individual Golgi stacks together to move in clusters. However, tubules detached from the Golgi were never observed. The fact that all correlation studies between ER marker fluorescence and ERD2-labelled Golgi fluorescence yielded a total lack of co-localization (Supplemental Figure 4) indicated that these tubules are not simply a portion of the ER network but may form part of a separate network that connects individual Golgi bodies (illustrated in Figure 8G). Investigations into the significance of Golgi tubules were beyond the scope of this study.

Golgi-residency of ERD2 depends on a di-leucine motif at the cytosolic C-terminus

A functional dissection of human ERD2 by site-directed mutagenesis (Townsley et al., 1993) revealed no specific residue at the C-terminus involved with ERD2 function. By contrast, phosphorylation of serine 209 in the human ERD2 C-terminus was proposed to be required for Golgi to ER transport (Cabrera et al., 2003). This serine residue is not conserved in eukaryotes including land plants (Figure 9A), but the fact that C-terminal fusions compromised the in vivo activity of plant ERD2 (Figures 4C, 5C) hints at an important function of its C-terminus. Since our bio-essay potentially reports on all aspects of ERD2 function, including the anterograde transport from the ER to the Golgi, we decided to investigate the influence of specific point-mutations in this region. Figure 9B shows that two conserved Leucine residues were important in maintaining the strong effect of untagged ERD2 in reducing Amy-HDEL secretion. Replacing both residues by glycine (LLGG) resulted in a strong inhibition of ERD2 activity in the bio-assay (Figure 9B, last lane).

To test if this lack of ERD2 activity is associated with a transport defect, the LLGG mutation was introduced to the active fluorescent ERD2 fusion (YFP-TM-ERD2-LLGG) and co-expressed in tobacco leaf epidermis with either the wild-type ERD2 fusion RFP-TM-ERD2 (Figure 9C) or the Golgi marker ST-RFP (Figure 9D). The data illustrate that the LLGG mutant fusion still reached the Golgi, but similar to the inactive C-terminal fluorescent fusions studied earlier (Figures 4C, 5C), a significant portion of YFP-TM-ERD2-LLGG was detected in the ER.

To test if the LLGG mutant exhibits any weak residual biological activity, we repeated the experiment from Figure 9B with higher amounts of GUS reference plasmids and compared wild-type ERD2 with ERD2-LLGG. Supplemental Figure 5 shows that ERD2-LLGG only mediated a very weak increase in amy-HDEL retention at the highest plasmid concentration. This shows that the LLGG mutation is not a complete knockout, but it is weak by comparison with YFP-TM-ERD2 and RFP-TM-ERD2 which show a clear effect even at the lowest plasmid concentration (Figure 5D).

We also carried out the same over-dose experiment for ERD2-YFP, since our data are in conflict with earlier published data (Montesinos et al., 2014) and we wanted to test for weak residual activity. Supplemental Figure 5 shows that even at the highest plasmid concentration ERD2-YFP did not show biological activity as judged by amy-HDEL secretion. The discrepancy

may be caused by the difference in methods, i.e. gel-loading and immunoblotting versus quantitative enzyme activity assays.

Finally, to illustrate the importance of the C-terminus, we created a deletion mutant that lacked the last predicted TM domain and the cytosolic tail of ERD2 (YFP-TM-ERD2-ΔTM7). When expressed in tobacco leaves, this fusion protein was exclusively found at the ER (Figure 9E). Together with the localization of YFP-ERP1 (Figure 5C), this shows that exclusive Golgi localization of our fusion proteins and the lack of ligand-induced re-distribution to the ER is not caused by a dominant Golgi localization signal from the additional TM domain of ERP1. This is also supported by the fact that Golgi residency as well as the tubular extensions were also observed with secYFP-ERD2 (Figure 4E), which does not have an extra TM domain.

Together, the data explain why C-terminal ERD2 fusions are non-functional and suggest that the dual ER-Golgi localization consistently reported in the literature may not reflect a biologically meaningful steady state distribution of functional ERD2. Our results indicate that the ERD2 C-terminus is essential for its biological function as well as its Golgi residency.

DISCUSSION

To help elucidate the role of ERD2 in cargo trafficking between the ER and the Golgi apparatus, it was important to establish probes that permit distinction between the individual transport steps involved. Ideally, functional studies should be able to trace both ligands and receptors *in vivo*. Here we have successfully established new tools to do so and identified unexpected transport properties of ERD2.

Gain-of-function assays reveal functional conservation of ERD2 between *Arabidopsis thaliana* and *Nicotiana benthamiana*

We show that ectopic expression of ERD2 leads to a sensitive dose-dependent activity assay in which ERD2 prevents secretion of Amy-HDEL without affecting constitutive Amy secretion (Figure 1E). This ERD2 gain-of-function assay is specific, sensitive and quantitative, using ectopic ERD2 expression levels beyond those causing a collapse of the Golgi (Hsu et al., 1992), as illustrated by a normal punctate Golgi morphology in transfected protoplasts (Figure 1F).

The assay also established that the two *ERD2* genes of *Arabidopsis thaliana* (*ERD2a* and *ERD2b*) show the same dose-response for HDEL- and KDEL-tagged Amy (Figure 2A,B), which can be considered as functional equivalents. Cross-species conservation was established with antisense-inhibition knockdown via a hybrid *Nicotiana benthamiana ERD2* (Figure 2C) which was shown to be functional when expressed by a sense transcript, inhibited ER retention when expressed as anti-sense, to be complemented by expression of sense Arabidopsis *ERD2b* in *Nicotiana benthamiana* cells (Figure 2D). The presence of two highly conserved *ERD2* genes in plants as diverse as *Arabidopsis thaliana*, *Nicotiana benthamiana*, *Oryza sativa*, *Selaginella moellendorffii* and *Physcomitrella patens* suggests that *ERD2* gene duplication is common in plants.

A new assay for ERD2 function *in situ*

To study ERD2 function *in situ*, we created a new fluorescent cargo based on the Golgi marker ST-YFP. This marker has a type II single membrane spanning topology with the YFP portion exposed to the lumen of the Golgi apparatus (Figure 3A). Tagging by the HDEL peptide resulted in a complete ER retention (Figure 3B), which can only partially fail when Amy-HDEL is overexpressed to saturate endogenous ERD2 (Figure 3B), resulting in a dual ER/Golgi labelling by ST-YFP-HDEL (Figures 3B, 3C). The partial accumulation at the Golgi apparatus can be abolished by co-expressing ERD2 in the same cell, leading to exclusive ER localization of ST-YFP-HDEL despite Amy-HDEL overexpression (Figure 3D).

It is important to understand the dynamic differences between the *in situ* assay (Figure 3) and the biochemical cell transport assay (Figures 1,2). Both assays directly report on the ability of ERD2 to prevent specific cargo molecules from accumulating outside the ER. Whilst Amy-HDEL permits quantitative dose-response assays, the visual ST-YFP-HDEL cargo illustrates the ER retention capability directly, albeit in a more qualitative manner. If Amy-HDEL dosage saturates endogenous ERD2, it leads to secretion of the cargo molecule to the culture medium, essentially a point of no return as it is diluted in the culture medium. The sensitivity of the cell retention assay is high because Amy-HDEL is highly stable in the culture medium. Even a small reduction of Amy-HDEL in the culture medium and an associated increase in the cells can be measured accurately in function of ERD2 co-expression.

Since ST-YFP-HDEL is membrane spanning, it cannot escape from the cells, which makes it an ideal molecule for microscopy. The Golgi-accumulating properties are contained within the

cytosolic N-terminus and transmembrane domain of the molecule (Boevink et al., 1998) and are independent on the nature of the fluorescent protein added. The fact that HDEL tagging of the lumenal YFP causes such dramatic ER retention (Figure 3B) indicates that ERD2 action takes precedence over the mechanisms leading to Golgi localization of ST-YFP. However, if ERD2-mediated ER retention is saturated, ST-YFP-HDEL remains in the Golgi, which is much easier to detect than diffuse apoplastic deposition of a soluble cargo.

The *Sec20* gene product is a naturally occurring type II membrane spanning protein with an HDEL signal for ER retention (Sweet and Pelham, 1992), but it appears to be a rare ER-retention strategy for membrane proteins in nature. One of the possible reasons could be that continuous recycling could lead to a buildup of such molecules and lead to saturation of ERD2, which would be toxic to the cell (Townsley et al., 1994).

ERD2 has an asymmetrical membrane topology

Systematic C-terminal and N-terminal extension experiments combined with protease protection and glycosylation assays (Figures 4, 5, 6) support an asymmetrical membrane topology model with a lumenal N-terminus and a cytosolic C-terminus (Lewis and Pelham, 1990; Townsley et al., 1993). Recent alternative models proposing an even number of transmembrane domains with both termini exposed at the cytosolic side (Singh et al., 1993; Brach et al., 2009) may have been influenced by changes to the ERD2 core structure, caused by fusions or modifications. It has been shown before that C-terminal and N-terminal protein fusions can lead to different subcellular localisations of membrane proteins (Gao et al., 2012). In this respect, it should be noted that experiments with redox-sensitive GFP fused to ERD2 (Brach et al., 2009) did not include subcellular localisation data that may have revealed the differences between C-terminal and N-terminally tagged ERD2 as observed here (Figure 4).

Membrane insertion of multiple membrane spanning proteins is thought to be guided by charge distributions of the first transmembrane domain (vonHeijne, 1989). However, folding of the N-terminus is also thought to be important (Spiess, 1995), in particular if the N-terminus is to be translocated to the ER lumen. Native ERD2 exhibits an extremely short N-terminus prior to the first predicted transmembrane domain. Introducing an entire fluorescent protein to this N-terminus (YFP-ERD2) may trap the molecule in the wrong orientation by a folded or partially YFP protein prior to translocation of the first transmembrane domain (Spiess, 1995). The

positively charged lysine residue at the end of the YFP coding region may seal this fate according to the positive-inside rule (vonHeijne, 1989).

The best labelling strategy can only be determined by trial and error (Snapp, 2005), and should be combined with an assay for in vivo activity. Our results illustrate that extending the ERD2 N-terminus with YFP only resulted in high expression and ER export when either a signal peptide was included in front of YFP or an additional transmembrane domain after YFP, both ensuring a lumenal N-terminus of ERD2. However, only the latter (*Y/R*FP-TM-ERD2) was biologically active as measured by their ability to increase the efficiency of HDEL-mediated protein retention (Figure 5, 7).

Functional fluorescent ERD2 fusions reside mainly at the early cisternae of the Golgi stacks

Subcellular localization of the fusion proteins (YFP-TM-ERD2 and RFP-TM-ERD2) revealed very sharp Golgi fluorescence with no evidence for detectable levels in transit through the ER network (Figures 5, 7, 8). ERD2 was also totally undetectable in the TGN when highlighted by the marker YFP-SYP61 (Figure 7E). Instead, the new ERD2 fusions accumulated at the Golgi bodies, except for a partial segregation from the trans-Golgi marker ST-RFP, observed by conventional CLSM (Figure 7D) and more clearly by high-resolution Airyscan (Figure 8B).

We also detected tubular emanations from the Golgi that were thinner than typical ER tubules and generally harder to see, requiring high detector gain settings and high magnification. They were seen with either non-functional secYFP-ERD2 (Figure 4E) or functional *Y/R*FP-TM-ERD2 (Figure 8B) and they co-localized with the Golgi but not ER markers (Figure 7A,B), suggesting that these tubules are distinct from the nearby ER network. Two or more adjacent Golgi bodies were found to be tethered together by such tubules whilst they move (Supplemental Movie 1). Figure 8G describes a model in which Golgi cisternae, and most likely the cis-cisternae, are held together by thin membrane tubules rich in ERD2, which may run in parallel to ER tubules but which do not overlap. Golgi tubules have been described in mammalian cells (Martínez-Alonso et al., 2013; Bottanelli et al., 2017) but their significance in Golgi function remains unknown. Native ERD2 has also been seen in Golgi tubules from mammalian cells after recovery from BFA treatment (Tang et al., 1993) but further work is necessary to characterize Golgi tubules in plants.

Predominant Golgi localization is important for ERD2 function

The recycling of sorting receptors has been a plausible explanation for how few receptors can mediate the transport of many ligands. The discovery that KDEL tagging promoted accumulation of cathepsin D in the ER but that it continued to undergo Golgi-modifications by mannose-6-phosphate-forming enzymes provided a compelling case for recycling. In plants, the observed dual localization of C-terminal fluorescent ERD2 fusions (Boevink et al., 1998) was therefore generally accepted. Here we show that a C-terminal fusion (ERD2b-YFP) lacks biological activity and fails to reduce secretion of amy-HDEL (Figures 4B, Supplemental Figure 5). This is in contrast to an earlier study in which ERD2a-YFP reduced the secretion of the reporter GFP-HDEL (Montesinos et al., 2014). Even though ERD2a and ERD2b appear to have the same function, it is possible that the former tolerates C-terminal fusions better than the latter. Another difference is the presence of the linker peptides between the *ERD2* coding regions and the *YFP* coding regions (the tri-peptide STF in ERD2a-YFP and the tetrapeptide ASAM in ERD2b-YFP). This can be tested experimentally in the future using any passenger protein harbouring a C-terminal HDEL or KDEL signal.

The critical importance of a native ERD2-C-terminus is illustrated by the fact that partial ER retention is probably caused by masking of the ERD2 C-terminus. Two conserved leucines in the tail are important for both Golgi residency and biological activity (Figure 9). This indicates that the ERD2 C-terminus plays a role in its own Golgi localization as well as its ability to mediate ER retention of its ligands.

The di-leucine motif appears to be unrelated to any earlier described Golgi localization signals such as the C-terminal KXD/E motif (Gao et al., 2012). The shift in steady state levels of the LLGG mutant (Figure 9D) could be caused by defective ER export, or accelerated Golgi-to-ER recycling. However, it is difficult to explain how faster recycling would lead to the drastic reduction in biological activity (Figure 9B; Supplemental Figure 5).

Interestingly, using the biologically active YFP-TM-ERD2 reporter, we were unable to show a ligand-induced ERD2-redistribution to the ER in epidermis cells (Figures 7B, 8D,E). A maximal ligand to receptor ratio was generated by combining a strong promoter-driven HDEL cargo with a weak promoter receptor fusion (Supplemental Methods 2) for multi-copy expression from the same plasmid vector (Figure 8D, E, F). In spite of this, YFP-TM-ERD2 remained in punctate structures even though Amy-HDEL was overexpressed to saturating levels (Figure 8F). These results are in conflict with an earlier report (Montesinos et al., 2014) based on C-terminally

652 tagged ERD2a-YFP similar to our construct in Figure 4C and internally tagged ERD2 (Li et al.,
653 2009), which we have tested as well (Supplemental Figure 3). The authors showed that these
654 ERD2 fusions undergo HDEL-ligand mediated redistribution back to the ER. The discrepancy
655 may be due to differences between ERD2a-YFP (Montesinos et al., 2014) and ERD2b-YFP
656 (this study) as discussed above, which can be tested by direct comparison against a common
657 denominator (i.e. the Golgi-marker ST-RFP). Although the internally tagged ERD2 used in this
658 study (E-YFP-RD2) has an identical primary sequence as the construct reported earlier (Li et
659 al., 2009, Montesinos et al., 2014), we could not observe Golgi localisation in any of our
660 expression systems. It cannot be ruled out that the presence of introns and the native *ERD2*
661 promoter from Arabidopsis promotes expression and Golgi localization in *Nicotiana*
662 *benthamiana* leaves and this can be tested by direct comparison against the Golgi-marker ST-
663 RFP.
664 A ligand-induced redistribution of ERD2 from the Golgi to the ER was initially proposed as
665 evidence for the receptor recycling principle (Lewis and Pelham, 1992). However, this effect
666 was not reproduced with stable transformed lines producing KDEL proteins in mammalian cells
667 (Tang et al., 1993). The authors only observed a shift of ERD2 from a perinuclear Golgi pattern
668 to a more diffuse pattern in transfected COS cells overexpressing ligands, but also suggested
669 that the identity of the diffuse pattern as ER was not established (Tang et al., 1993). It cannot
670 be excluded that ER-like patterns observed in earlier studies (Lewis and Pelham, 1992) could
671 be due to C-terminal tagging. Alternatively, an ER-retained ERD2 pattern may also have been
672 caused by ERD2 overexpression which was shown to strip Golgi-membranes of coatomer
673 (COPI), leading to a Brefeldin A-like effect (Hsu et al., 1992). Although KDEL receptors have
674 been detected by immunogold labeling in COPI-coated buds and vesicles (Griffiths et al.,
675 1994), the ERD2-mediated recruitment of ARF-GAP (Aoe et al., 1997) and associated
676 dissociation of COPI from the Golgi (Hsu et al., 1992) appears to be at odds with its recycling
677 function.
678 Our results do not exclude the possibility that ERD2 cycles through the ER so quickly that it
679 escapes detection. Likewise, in the presence of an active ERD2 fusion, HDEL cargo in transit
680 through the Golgi was below the detection limit even when ST-YFP-HDEL was co-expressed
681 with amy-HDEL (Figure 7B). Finally, it is possible that ER retention in plants and mammals
682 occurs via different mechanisms, since the latter contain a separate ER-Golgi intermediate
683 compartment (ERGIC) which has not been found in plants (Appenzeller-Herzog and Hauri,

2006). In addition, it is noteworthy that the ER resident glyco-protein calreticulin was found to be fully endoH-resistant and thus of the high mannose type when extracted from cells, despite 100-fold overexpression (Crofts et al., 1999). The drastic overexpression caused formation of dilated globular ER domains filled with calreticulin and also causing partial secretion of a small proportion of calreticulin due to saturation of the retention machinery. Only the secreted portion of calreticulin from the culture medium was endoH-resistant, not the intracellular calreticulin which represented the vast majority of the total. This indicates that retrograde transport of Golgi-modified HDEL proteins back to the ER has yet to be demonstrated in plants and cannot be simply assumed.

Conclusions

We have established an asymmetrical topology of ERD2 and created a new fluorescent ERD2 fusion that retains biological activity. Unexpectedly, the fusion appears to be Golgi resident and cannot be detected in the ER regardless of ligand overexpression. Golgi residency as well as biological function depend on a conserved di-leucine motif interrupted with a non-conserved amino acid (LXL) near the ERD2 C-terminus which does not resemble any known targeting signals. Further work is needed to establish how ERD2 mediates ER retention of its ligands, but the mechanism appears to be highly efficient. If a recycling mechanism is operating it must include a very fast ERD2 transport route back to the Golgi, well in excess of the bulk flow rate by which soluble proteins leave the ER. The gain-of-function assays developed in this study will be instrumental in identifying the individual steps of the ERD2 transport cycle in future.

METHODS

Recombinant DNA constructs

All plasmids were grown in *Escherichia coli* strain MC1061 (Casadaban and Cohen, 1980) using standard procedures involving the generation of transformation competent cells, growth on solid and in liquid media as well as routine DNA purification techniques. Recombinant plasmids were built via conventional well-established molecular biology techniques involving either restriction and ligation, PCR amplification and assembly or complete gene synthesis. A complete list of plasmids used in this study is shown in Supplemental Table 1. Maps and

716 relevant gene structures of the main expression plasmids are provided in Supplemental
717 Methods 1 and 2, and the construction of further derivatives is described below.
718
719 **Cargo plasmids**
720 Plasmids encoding cargo proteins for biochemical transport assays in protoplasts
721 (Supplemental Methods 1, Supplemental Table 1) contain the strong CaMV35S promoter
722 flanked between EcoRI and NcoI, followed by the barley α-amylase coding region and the 3'
723 untranslated end of the nopaline synthase gene (3'nos) used before (Crofts et al., 1999;
724 Phillipson et al., 2001). Sequence modifications for derivatives Amy-HDEL and Amy-KDEL
725 containing different ER retention motifs are disclosed in Supplemental Methods 1.
726 The sequence encoding the C-terminus of calreticulin was amplified via PCR from pLC48
727 (Crofts et al., 1999) to generate Amy-cal (pOF12) and Amy-calΔHDEL (pOF8) as described in
728 Supplemental Methods 1.
729 For *in situ* experiments with ER retention, the Golgi marker ST-YFP coding region was
730 amplified from pTFB62 (Bottanelli et al., 2012) was modified by PCR amplification using styfp-
731 sense (5'-CACCAAATCGATGATTCATACCAACTTGAAG-3') and YFP-HDEL-anti
732 (5'GGTTACACTCTAGACTAGAGTTCATCATGGTCCTCCTTGTACAGCTCGTCCATGC
733 CGAG-3') to yield the ST-YFP-HDEL coding region, which was inserted as ClaI-BamHI
734 fragment to replace ST-YFP in pTFB62 under the transcriptional control of the TR2' promoter
735 (pTJA15). HDEL competition experiments were carried out with dual expression vectors in
736 which the PAT coding region under the transcriptional control of the CaMV35S promoter was
737 replaced by either Amy (pTJA34) or Amy-HDEL (pTJA35) coding regions, illustrated in
738 Supplemental Methods 1.
739
740 **ERD2 plasmids**
741 The coding regions of *ERD2a* (AT1G29330) and *ERD2b* (AT3G25040) were obtained via gene
742 synthesis introducing a ClaI site overlapping with the start codon and XbaI site following the
743 stop codon yielding the sequences illustrated in Supplemental Methods 2 and placed under the
744 transcriptional control of the CaMV35S promoter in the dual expression vector together with
745 TR2'-ST-CFP-3'ocs as internal marker (pAG10 and pAP10). The CaMV35S:ERD2a-3'nos and
746 CaMV35S:ERD2b-3'nos construct was also cloned in a pUC19 vector on its own (yielding
747 pAG2 and pAG3 respectively). CaMV35S:ERD2b-3'nos was also cloned into pGUSref

(Gershlick et al., 2014) yielding pJA31 and into an *Agrobacterium tumefaciens* dual expression vector (pTJA36), maps of which are shown in Supplemental Methods 2.

C-terminal fluorescent fusions of ERD2a and ERD2b were generated by introducing an NheI site overlapping with the last codon of *ERD2a* or *ERD2b*, using anti-sense primers ERD2a-NheI (5'-CATTGCGCTAGCCGGAAGCTTAAGTTTGGTGTTGG-3') and ERD2b-NheI (5'-TCATTGCGCTAGCAGCTGGTAATTGGAGCTTTTTGTTG-3') in conjunction with the sense primer cool35S (5'-CACTATCCTTCGCAAGACC-3') using pAG2 or pAG3 as templates. To obtain a matching YFP coding region for in-frame fusion, the *YFP* coding region was amplified with primers NheI-YFP (5'-TACCAGCTGCTAGCGCAATGAGCAAGGGCGAGGAGCTG-3') and YFP-anti (5'- GGATCCTCTAGACTACTTGTACAGCTCGTCCATGCC-3') using pFB62 as template. The ClaI-NheI ERD2a or ERD2b fragments were then ligated together with the NheI-XbaI YFP fragment into pJA31, cut with ClaI and XbaI and dephosphorylated, to yield pAP11 and pJA47. ERD2-RFP was created in a similar way, except that primer Nhe1-RFP (5'-CCAGCTGCTAGCGCAATGGCCTCCTCCGAGGAC-3') and RFP-anti (5'-TCTGCTTCGGATCCCTATGCGCCGGTGGAGTGGCGGCCC-3') were used with Aleu-RFP (Bottanelli et al., 2011) as template. A ClaI-NheI ERD2b fragment and an NheI-BamHI RFP fragment were then inserted together in pAG3, cut with ClaI and BamHI and dephosphorylated, to yield pAG8.

YFP-ERD2b was constructed by cutting pOF21 (Foresti et al., 2006) with EcoRI-ClaI to extract 35S:YFP, which was ligated into pJA31, cut with EcoRI-Cla1 and dephosphorylated, to yield pJA51. A signal peptide and glycosylation peptide was added to generate secYFP-ERD2b by extracting an EcoRI-NcoI fragment from pLL50 (Foresti et al., 2006) and amplifying pJA51 with primer YFP/NcoI-sense (5'-CTGCCCGTGCCATGGCCCACCCTCGTGACCACC-3') and pUCOF from which an NcoI-HindIII fragment was extracted. Both fragments were ligated together into pJA31, cut with EcoRI-HindIII and dephosphorylated, to yield pJCA17. To generate secYFP-ERD2b-RFP, we extracted an EcoRI-KpnI fragment from pJCA17 and ligated it into pAG8, cut with the same two enzymes and dephosphorylated, to yield pJA72.

E-YFP-RD2 was generated by assembly-PCR to introduce a YFP coding region between the first and the second predicted transmembrane domains of ERD2b as described (Li et al., 2009), except for the omission of an intron and the use of either the CaMV35S promoter (pFLA114) or the *TR2* promoter (pTFLA115) instead of the *Arabidopsis thaliana ERD2b* promoter. The sequence of the hybrid coding region is shown in Supplemental Methods 2.

An *ERD2* hybrid sequence containing the first half of *Nicotiana benthamiana ERD2a* (Niben101Scf05948g07012.1) and the second half of *Nicotiana benthamiana ERD2b* (Niben101Scf08478g05002.1) was obtained by gene synthesis as described in Supplemental Methods 2. For sense expression, the hybrid sequence was cut out as a ClaI-XbaI fragment and ligated into pJA31, to yield pJCA59. For anti-sense expression, the hybrid sequence was cut out with NcoI-BamHI and inserted into pJA51, to yield pJCA60.

ERP1 construct

The coding region of *AtERP1* (AT4G38790) was obtained via gene synthesis introducing a ClaI site overlapping with the start codon and XbaI site following the stop codon yielding the sequences illustrated in Figure 5, which was inserted as ClaI-XbaI fragment into pTFLA32 under the transcriptional control of the *TR2'* promoter (pTFLA27) to create the YFP-ERP1.

ERD2 with additional transmembrane domains

To add a transmembrane domain between the C-terminus of ERD2b and RFP, the sequence (ERD2b-TM) was synthesized and described in Supplemental Methods 2. The sequence was trimmed by ClaI-NheI and ligated into pAG8, cut with the same enzymes and dephosphorylated, to yield pFLA93 encoding ERD2b-TM-RFP. The resulting hybrid coding region was also ligated as a ClaI-BamHI fragment into pJA31, cut with the same enzymes and dephosphorylated, to yield pFLA72. To generate secYFP-ERD2-TM-RFP, pFLA72 was cut with EcoRI-KpnI and dephosphorylated, and ligated to an EcoRI-KpnI fragment extracted from pJCA17, to yield pFLA92.

To insert a transmembrane domain and cytosolic linker between YFP and ERD2b, the sequence (TM-ERD2b) was synthesized and described in Supplemental Methods 2. The sequence was trimmed with ClaI-XbaI and inserted either into pJA51 cut with the same enzymes and dephosphorylated, to yield pFLA30 encoding YFP-TM-ERD2b. The same fragment was inserted into pJA31 using the same strategy, to yield pFLA33 encoding TM-ERD2b. To generate RFP-TM-ERD2b (pFLA40), we amplified the *RFP* coding sequence using NcoI-RFP (5'- TCTATAACCATGGCCTCCTCCGAGGACGTC-3') and RFP-ClaI (5'-CGCCTTCATCGATGCGCCGGTGGAGTGGCGGCCCTC-3') from pAG8 as template, trimmed the PCR product with NcoI-ClaI and replaced the *YFP* coding region in pFLA30 using the same sites.

812

813 **Fluorescent ERD2 fusions**

814 For sub-cellular localization studies, fluorescently tagged ERD2 constructs described above
815 were also sub-cloned into *Agrobacterium tumefaciens* plant expression vectors pGSC1700
816 (Cornelissen and Vandewiele, 1989) or pDE1001 (Denecke et al., 1992) between EcoRI-
817 HindIII. This results in plasmids where the relevant coding regions remain under the
818 transcriptional control of the CaM35S promoter, including ERD2a-YFP (pTAP11), ERD2b-YFP
819 (pTJA10), YFP-ERD2b (pTOF122), secYFP-ERD2b (pTJCA24), and secYFP-ERD2b-RFP
820 (pTCSJ1).
821 For sub-cellular localization studies at low expression, chimeric coding regions were subcloned
822 under the transcriptional control of the weak *TR2* promoter. For this purpose, pTFB62 was cut
823 with ClaI-HindIII, followed by dephosphorylation, to be used as vector. The ERD2b-TM-RFP-
824 3'nos fragment was extracted from pFLA72 by a complete ClaI-HindIII digest to yield pTFLA94
825 after ligation to the vector. The secYFP-ERD2-3'nos fragment was obtained by partial ClaI and
826 complete HindIII digest, to yield pTFLA25. Other fluorescent ERD2 fusions had an NcoI site at
827 the start codon of the chimeric coding region and we generated a *TR2* promoter fragment by
828 PCR amplification using primers PUCsense (5'-
829 AAAACTCATCGATGATGGGCCGGATCTTTG-3') and TR2:NcoI (5'-
830 CTTGCTCACCATGGATTTGGTGTATCGAGATTGGTTATG-3') and pAG10 (Supplemental
831 Methods 2) as template. The PCR product was digested using EcoRI-NcoI to yield the new
832 *TR2* promoter fragment. Plasmids pFLA30 and pFLA40 were digested using NcoI and HindIII
833 to yield fragment YFP-TM-ERD2b-3'nos, and RFP-TM-ERD2-3'nos and ligated together with
834 the promoter fragment into pDE1001 cut with EcoRI-HindIII and dephosphorylated to yield
835 pTFLA32 and pTFLA41 (Supplemental Table 1).

836

837 **Mutagenesis and deletions**

838 Point mutations of the C-terminus of AtERD2b were created via the standard quick change
839 method and resulted in codon changes to yield amino acid substitutions as indicated in Figure
840 9.
841 YFP-TM-ERD2-ΔTM7 was generated by PCR using an anti-sense primer ERD2-ΔTM7 (5'-
842 ATCCAGTGGCTAGCGTGCGGCTCAGTGAAGTAACGGTA-3') combined with cool35S (5'-
843 CACTATCCTTCGCAAGACC-3') using pFLA30 as template. The ClaI-NheI YFP-TM-ERD2-

ΔTM7 fragment was then ligated together with NheI-HindII 3'nos fragment cut from pFLA98 into pTFB62, cut with ClaI-HindIII, followed by dephosphorylation, to yield pTFLA106.

Organelle markers

The Golgi-marker ST-RFP was based on *Agrobacterium tumefaciens* dual expression vector similar to pTFB62 (Bottanelli et al., 2012), except that *YFP* was replaced by *RFP* in the ST-YFP coding region, yielding pTJA37. Previously published organelle markers were the CaMV35S:YFP-SYP61 fusion used as TGN marker (Foresti et al., 2010) and CaMV35S:RFP-HDEL as ER marker (Gershlick et al., 2014).

Triple expression vector

A map of the triple expression vector is shown in Supplemental Methods 2 encoding a unique fluorescently tagged and biologically active ERD2b fusion (YFP-TM-EDR2) under the transcriptional control of the pNOS' promoter bearing an internal marker GUS under the transcriptional control of the *TR2'* promoter and either Amy (pFLA43) or Amy-HDEL (pFLA44) under the transcriptional control of the strong CaMV35S promoter. These constructs were made by several complicated steps, the detailed description of which would take us well beyond the word limit of this manuscript. For the interested reader, it involved combining gene structures of pGUSRef (Gershlick et al., 2014), the insertion of Amy or Amy-HDEL coding regions under the control of the CaMV35S promoter, elimination of unnecessary inconvenient restriction sites, gene synthesis of the *Arabidopsis thaliana ADH* 3'end (AT1G77120) carrying a polyadenylation signal and a polylinker as well as the modification of the nopaline synthase promoter from pDE1001 to exhibit an NcoI site overlapping with the start codon for ligation to the chimeric YFP-TM-ERD2b coding region of pFLA30. This resulted in a new triple expression vector, a detailed restriction map of which is shown in Supplemental Methods 2. The plasmid will be made available together with the complete sequence upon request.

Plant material and standard transient protoplast expression procedure

Sterile grown *Nicotiana tabacum* cv., Petit Havana (Maliga et al., 1973) and *Nicotiana benthamiana* (Goodin et al., 2008) plants were grown from surface-sterilized seeds. Typically, 20 mg seeds were incubated for 30 minutes in 1 ml of 10% bleach supplemented with 0.1% Tween 20 in a microfuge tube, washed 5-fold with 1 ml autoclaved distilled water, followed by

placing on the surface of Murashige and Skoog medium (Murashige and Skoog, 1962) supplemented with 2% sucrose and incubated in a controlled room at 22°C with a 16-h day length at a light irradiance of 200 mE/m^2/second (standard white Osram L36 W/23 fluorescent tube). After 2 weeks incubation, individual seedlings are lifted out and planted individually in glass jars for a further 3-6 week incubation under the same conditions to create sufficient sterile leaves for transient expression analysis. Preparation of tobacco leaf protoplasts and standard transient expression analysis via electroporation, protoplast incubation, harvesting cells and medium were done as described previously (Foresti et al., 2006; Gershlick et al., 2014), except that sterile *Nicotiana benthamiana* plants were used. For anti-sense inhibition and complementation analysis, protoplasts were incubated for 48 hours.

Drug treatments

To test for N-linked glycosylation, two standard protoplast electroporations were pooled, divided into equal portions, one to be supplemented with Tunicamycin to a final concentration of 10µg/mL suspension whilst the control received the same amount of solvent-only (DMSO).

Protein Extraction

Proteins were extracted from protoplasts pelleted in 250mM NaCl as described before (Foresti et al., 2006) using specific buffers and procedures depending on the type of experiment.

In order to measure α-amylase activities and also detect the internal marker ST-CFP by SDS-PAGE, the pellets remaining after protoplast sonication with amy-extraction buffer, centrifugation and recovery of the supernatant for standard amy-assays (Foresti et al., 2006) were kept to be extracted again by sonication in 250 µL membrane protein extraction (MPE) buffer (100 mM Tris-HCl, pH 7.8, 200 mM NaCl, 1 mM EDTA, 0.2% Triton X-100, and 2% β-mercaptoethanol), followed by 10-min centrifugation at 19,745g at 4°C and subsequent recovery of the supernatant to be mixed 50:50 with SDS-PAGE sample buffer (see below).

For combined GUS-normalised effector dose-response assays (Gershlick et al., 2014), 2.5 ml protoplast suspension from a standard electroporation were divided into a 500 µL sample for GUS analysis and a 2000 µL sample kept in a conical 10mL tube for Amy analysis. The GUS sample was immediately mixed with 500 µL of GUS extraction buffer [50mM (P) Sodium buffer pH 7.0; 10mM Na2EDTA; 0.1% sodium lauryl sarcosine; 0.1% Triton X-100 and 10 mM β-Mercaptoethanol] and transferred to ice. The mixed GUS extraction samples on ice (1 ml) were

first sonicated (60% for 5s), vortexed and centrifuged at 14,000 rpm (Sigma 12132 rotor) and 4°C for 15 minutes, after which 500 µL supernatant was recovered and kept on ice. The amy sample was centrifuged to recover cell-free medium as well as washed cells and all further steps to measure cellular and secreted α-amylase activity measurement as described before (Foresti et al., 2006), but implementing volumetric calculations based on 2mL total suspension, rather than the standard 2.5 ml.

For standard SDS-PAGE of ERD2 fusion proteins, cell pellets were extracted in MPE buffer. For protease-protection experiments, washed cell pellets from a standard 2.5 mL transiently expressing cell suspension (Foresti et al., 2006) were resuspended in 300 µL of ice-cold homogenization buffer (50 mM TRIS-HCL pH 8, 10 mM KCl, 1 mM EDTA pH 8, 12% sucrose), and transferred to a borosilicate mini homogenizer for cell shearing with a borosilicate pestle via 10 up-strokes and 10 down-strokes under continuous rotation. The homogenate was transferred to a 1.5-mL microfuge tube, centrifuged at 2000 g for 1 minute to remove large cell debris, after which the crude supernatant containing osmotically stabilized microsomes was transferred to ice for immediate further analysis.

SDS-PAGE and Gel Blot Analysis

Protein extracts were denatured using freshly prepared sucrose sample buffer (SSB). This buffer is based on a sample buffer mix (0.1% bromophenol blue, 5 mM EDTA, 200 mM Tris-HCl, pH 8.8, and 1 M sucrose) which is stored in 900 µL aliquots at -20°C. Immediately prior to use, an aliquot is thawed and supplemented with 300 µL of 10% SDS (kept at room temperature) and 20 µL of 1 M DTT (kept in aliquots at -20°C). Protein extracts are diluted 50:50 with SSB and denatured at 95°C for 5 min and loaded on 12% SDS-PAGE.

Separation gel contained 12% Protogel [30% acrylamide, 0.8% bisacrylamide; supplied by National Diagnostics], 420 mM Tris-HCl, pH 8.8, 0.1% SDS, 0.056% N,N,N9,N9-tetramethylethylenediamine (Temed), and 0.033% ammonium persulfate (APS). Stacking gels contained 5% Protogel, 15% sucrose, 66 mM Tris-HCl, pH 6.8, 0.1% SDS, 0.2% Temed, and 0.033% APS). All percentages are given in w/v ratios. Gels were run in running buffer (6 g/L Tris, 28.8 g/L glycine, and 1 g/L SDS), electroblotted on nitrocellulose membranes in blotting buffer (3 g/L Tris, 14.4 g/L Glycine and 10% Methanol) using standard procedures. For immunodetection we used rabbit polyclonal antiserum raised against GFP and RFP (ThermoFischer Scientific, PA5-22688 and R10367) at 1:5000 dilution, in conjunction with

peroxidase-labelled anti-rabbit IgG (Sigma, A0545) and home-made enhanced chemiluminescence (ECL) solution 1 (100 mM Tris-HCl, pH 8.5, 2.5 mM luminol, and 0.4 mM p-coumaric acid) and ECL solution 2 (100 mM Tris-HCl, pH 8.5, and 0.02% H_20_2).

Enzyme assays

Measurement of α-amylase activity and calculation of the secretion index (ratio of extracellular to intracellular enzyme activities) were done as described previously (Foresti et al., 2006; Gershlick et al., 2014). For GUS-normalised effector dose-response assays, the GUS enzyme essay was performed essentially as described earlier (Gershlick et al., 2014) but with the following modifications. To reduce the signal to noise ratio due to pigments present in the cell extracts, we took advantage of the extraordinary stability of the GUS enzyme and its substrate 4-Nitrophenyl-β-D-glucopyranosiduronic acid and performed the essay with 10-fold diluted extracts and longer incubation periods. 10 µl of the above described GUS extract was transferred into a 96-well microtitre plate and mixed with 90 µl of GUS extraction buffer and 100 µl of the GUS reaction buffer [50 mM (P) Sodium buffer pH 7.0; 0.1% Triton; 2 mM 4-Nitrophenyl-β-D-glucopyranosiduronic acid and 10 mM β-Mercaptoethanol]. These samples were then incubated at 37°C, typically for 16 hours, before being stopped with 80 µl of 2.5 M 2-amino-2methyl propanediol. As negative control, an extract from a mock-electroporated sample was analyzed in the same way. To avoid evaporation during the longer incubation period, the 96-well plate was covered with Aluminium Starseal tape. The optical absorbance was directly measured in the microtitreplate at λ405nm. The optical density (OD) measured for the mock sample was subtracted from the ODs measured from the corresponding sample test readings to yield ΔOD.

Microsomal protease protection

To determine the transmembrane topology of HDEL/KDEL receptor, ERD2b, osmotically stabilized microsomes were divided into three identical aliquots of 50 µL on ice. The Control tube (C) remained on ice. The Proteinase tube (K) was supplemented with 1µl of Proteinase K (5mg/ml) and incubated at 25^{o}C for 30 minutes and placed back on ice. The Proteinase+Triton sample (KT) was treated in the same way but with an additional 5 µl of triton at 10%. All samples were then supplemented with 2 µl of PMSF 0.5M and incubated for a further 10

minutes on ice. Samples were diluted with 50 µL of SSB and boiled at 95°C for 5 minutes for standard SDS-PAGE as described above.

Tobacco Leaf Infiltration Procedure

Soil-grown tobacco plants were infiltrated with overnight cultures of *Agrobacterium tumefaciens* cultures grown in MGL, diluted to an OD of 0.1 at 600 nm, and infiltrated into leaves of 5 week old soil-grown *N. tabacum* cv Petit Havana (Maliga et al., 1973) as described previously (Sparkes et al., 2006). CLSM analysis was done 48 hours after infiltration, unless otherwise indicated in the figure legends.

Fluorescence confocal microscope imaging and analysis

Infiltrated tobacco leaf squares (0.5 x 0.5 cm) were mounted in tap water with the lower epidermis facing the thin cover glass (22 x 50 mm; No. 0). Protoplasts were mounted on slides supplemented with 0.1 mm electrical tape with a cut-out square of 1 x 1 cm to create a well for the protoplast suspension between slide and cover glass, as described previously (daSilva et al., 2005, 2006). Confocal imaging was performed using an upright Zeiss LSM 880 Laser Scanning Microscope (Zeiss) with a PMT or a high-resolution Airyscan detector, a Plan-Apochromat 40x/1.4 oil DIC M27 objective or Plan-Apochromat 63x/1.4 oil DIC M27 objective.
When YFP-fusions were imaged alone, the excitation wavelength was 514 nm and fluorescence was detected with a bandpass filter 519-620 nm. When RFP-fusions were imaged alone, the excitation wavelength was 561 nm and fluorescence was detected with a bandpass filter 585-650 nm.
To image YFP-fusions together with RFP-fusions, samples were excited using an Argon ion laser at the wavelength of 488 nm for YFP and a HeNe ion laser at 561 nm for RFP. A 488/543 dichroic beam splitter was used to detect fluorescence, YFP fluorescence was detected with a bandpass filter 493-529 nm and RFP fluorescence was detected with a bandpass filter 585-650 nm. All dual color imaging was performed by line switching to obtain adequate live bio-imaging data that are not distorted by organelle motion.
Post-acquisition image processing was performed with the Zen 2.3 lite blue edition (Zeiss) and ImageJ ((http://rsb.info.gov/ij/)). Image analysis was undertaken using the ImageJ analysis program and the PSC co-localization plug-in (French et al., 2008) to calculate co-localization and to produce scatter plots as described before (Foresti et al., 2010).

Supplemental Data

Supplemental Figure 1. Alternative colors for the biological activity *in situ* of ERD2 from figure 3 (C,D, merged channels).

Supplemental Figure 2. Signal-peptide-mediated translocation of N-terminally fused YFP stabilises Golgi residency of ERD2.

Supplemental Figure 3: Internal tagging in the first cytosolic loop.

Supplemental Figure 4. RFP-TM-ERD2 does not co-localize with HDEL ligands.

Supplemental Figure 5. The C-terminus of ERD2 controls efficient ER export and is essential for its biological activity.

Supplemental Methods 1: Cargo plasmids

Supplemental Methods 2: Receptor constructs

Supplemental Table 1. Constructs used in this work.

Supplemental Movie 1: Golgi bodies connected by tubules

AUTHOR CONTRIBUTIONS

F.A.L.S.-A., J.A., J.C.A., O.F. and J.D. conceived and designed the research. All authors performed research and analyzed data. F.A.L.S.-A., J.C.A. and J.D. wrote the article.

ACKNOWLEDGMENTS

The work in this article was in part supported by the European Union (projects HPRN-CT-2002-00262 and LSH-2002-1.2.5-2), the Biotechnology and Biological Sciences Research Council (BBSRC) project nr. BB/D016223/1 and The Leverhulme Trust (F/10 105/E). Jonas C Alvim is grateful for a PhD scholarship awarded from the Conselho Nacional de Desenvolvimento Científico e Tecnológico – Brasil (CNPq 201192/2014-4). We thank Joe McKenna for advice and help with the airyscan system.

References

Aoe, T., Cukierman, E., Lee, A., Cassel, D., Peters, P.J., and Hsu, V.W. (1997). The KDEL

1035 receptor, ERD2, regulates intracellular traffic by recruiting a GTPase-activating protein for
1036 ARF1. EMBO J. 16: 7305–7316.
1037 Appenzeller-Herzog, C. and Hauri, H.-P. (2006). The ER-Golgi intermediate compartment
1038 (ERGIC): in search of its identity and function. J. Cell Sci. 119: 2173–83.
1039 Batoko, H., Zheng, H.Q., Hawes, C., and Moore, I. (2000). A rab1 GTPase is required for
1040 transport between the endoplasmic reticulum and golgi apparatus and for normal golgi
1041 movement in plants. Plant Cell 12: 2201–18.
1042 Boevink, P., Oparka, K., Cruz, S.S., Martin, B., Betteridge, A., and Hawes, C. (1998). Stacks
1043 on tracks: The plant Golgi apparatus traffics on an actin/ER network. Plant J. 15: 441–447.
1044 Bottanelli, F. et al. (2017). A novel physiological role for ARF1 in the formation of bidirectional
1045 tubules from the Golgi. Mol. Biol. Cell 28: 1676–1687.
1046 Bottanelli, F., Foresti, O., Hanton, S., and Denecke, J. (2011). Vacuolar transport in tobacco
1047 leaf epidermis cells involves a single route for soluble cargo and multiple routes for
1048 membrane cargo. Plant Cell 23: 3007–25.
1049 Bottanelli, F., Gershlick, D.C., and Denecke, J. (2012). Evidence for Sequential Action of Rab5
1050 and Rab7 GTPases in Prevacuolar Organelle Partitioning. Traffic 13: 338–354.
1051 Brach, T., Soyk, S., Müller, C., Hinz, G., Hell, R., Brandizzi, F., and Meyer, A.J. (2009). Non-
1052 invasive topology analysis of membrane proteins in the secretory pathway. Plant J. 57:
1053 534–541.
1054 Brandizzi, F. and Barlowe, C. (2013). Organization of the ER–Golgi interface for membrane
1055 traffic control. Nat. Rev. Mol. Cell Biol. 14: 382–392.
1056 Brandizzi, F., Snapp, E.L., Roberts, A.G., Lippincott-Schwartz, J., and Hawes, C. (2002).
1057 Membrane protein transport between the endoplasmic reticulum and the Golgi in tobacco
1058 leaves is energy dependent but cytoskeleton independent: evidence from selective
1059 photobleaching. Plant Cell 14: 1293–309.
1060 Cabrera, M., Muniz, M., Hidalgo, J., Vega, L., Martın, M.E., and Velasco, A. (2003). The
1061 Retrieval Function of the KDEL Receptor Requires PKA Phosphorylation of Its C-
1062 Terminus. Mol. Biol. Cell 14: 4114–4125.
1063 Cancino, J., Capalbo, A., Di Campli, A., Giannotta, M., Rizzo, R., Jung, J.E., Di Martino, R.,
1064 Persico, M., Heinklein, P., Sallese, M., and Luini, A. (2014). Control Systems of Membrane
1065 Transport at the Interface between the Endoplasmic Reticulum and the Golgi. Dev. Cell
1066 30: 280–294.

1067 Capitani, M. and Sallese, M. (2009). The KDEL receptor: new functions for an old protein.
1068 FEBS Lett. 583: 3863–71.
1069 Casadaban, M.J. and Cohen, S.N. (1980). Analysis of gene control signals by DNA fusion and
1070 cloning in Escherichia coli. J. Mol. Biol. 138: 179–207.
1071 Cornelissen, M. and Vandewiele, M. (1989). Nuclear transcriptional activity of the tobacco
1072 plastid psbA promoter. Nucleic Acids Res. 17: 19–29.
1073 Crofts, A., Leborgne-Castel, N., Hillmer, S., Robinson, D., Phillipson, B., Carlsson, L., Ashford,
1074 D., and Denecke, J. (1999). Saturation of the endoplasmic reticulum retention machinery
1075 reveals anterograde bulk flow. Plant Cell 11: 2233–48.
1076 Dacks, J.B., Poon, P.P., and Field, M.C. (2008). Phylogeny of endocytic components yields
1077 insight into the process of nonendosymbiotic organelle evolution. Proc. Natl. Acad. Sci.
1078 105: 588–593.
1079 daSilva, L.L.P., Foresti, O., and Denecke, J. (2006). Targeting of the Plant Vacuolar Sorting
1080 Receptor BP80 Is Dependent on Multiple Sorting Signals in the Cytosolic Tail. Plant Cell
1081 Online 18.
1082 daSilva, L.L.P., Snapp, E.L., Lippincott-schwartz, J., Hawes, C., and Brandizzi, F. (2004).
1083 Endoplasmic Reticulum Export Sites and Golgi Bodies Behave as Single Mobile Secretory
1084 Units in Plant Cells. Society 16: 1753–1771.
1085 daSilva, L.L.P., Taylor, J.P., Hadlington, J.L., Hanton, S.L., Snowden, C.J., Fox, S.J., Foresti,
1086 O., Brandizzi, F., and Denecke, J. (2005). Receptor Salvage from the Prevacuolar
1087 Compartment Is Essential for Efficient Vacuolar Protein Targeting. Plant Cell Online 17.
1088 Denecke, J., Rycke, R. De, and Botterman, J. (1992). Plant and mammalian sorting signals for
1089 protein retention in the endoplasmic reticulum contain a conserved epitope. EMBO J. 11:
1090 2345–2355.
1091 Dettmer, J., Hong-Hermesdorf, A., Stierhof, Y.-D., and Schumacher, K. (2006). Vacuolar H+-
1092 ATPase activity is required for endocytic and secretory trafficking in Arabidopsis. Plant
1093 Cell 18: 715–30.
1094 Foresti, O., daSilva, L.L.P., and Denecke, J. (2006). Overexpression of the Arabidopsis
1095 Syntaxin PEP12/SYP21 Inhibits Transport from the Prevacuolar Compartment to the Lytic
1096 Vacuole in Vivo. PLANT CELL ONLINE 18: 2275–2293.
1097 Foresti, O. and Denecke, J. (2008). Intermediate organelles of the plant secretory pathway:
1098 Identity and function. Traffic 9: 1599–1612.

1099 Foresti, O., Gershlick, D.C., Bottanelli, F., Hummel, E., Hawes, C., and Denecke, J. (2010). A
1100 recycling-defective vacuolar sorting receptor reveals an intermediate compartment
1101 situated between prevacuoles and vacuoles in tobacco. Plant Cell 22: 3992–4008.
1102 French, A.P., Mills, S., Swarup, R., Bennett, M.J., and Pridmore, T.P. (2008). Colocalization of
1103 fluorescent markers in confocal microscope images of plant cells. Nat. Protoc. 3: 619–628.
1104 Gao, C., Yu, C.K.Y., Qu, S., San, M.W.Y., Li, K.Y., Lo, S.W., and Jiang, L. (2012). The Golgi-
1105 localized Arabidopsis endomembrane protein12 contains both endoplasmic reticulum
1106 export and Golgi retention signals at its C terminus. Plant Cell 24: 2086–104.
1107 Gershlick, D.C., Lousa, C.D.M., Foresti, O., Lee, A.J., Pereira, E. a, daSilva, L.L.P., Bottanelli,
1108 F., and Denecke, J. (2014). Golgi-dependent transport of vacuolar sorting receptors is
1109 regulated by COPII, AP1, and AP4 protein complexes in tobacco. Plant Cell 26: 1308–29.
1110 Goodin, M.M., Zaitlin, D., Naidu, R.A., and Lommel, S.A. (2008). Nicotiana benthamiana : Its
1111 History and Future as a Model for Plant–Pathogen Interactions. Mol. Plant-Microbe
1112 Interact. 21: 1015–1026.
1113 Griffiths, G., Ericsson, M., Krijnse-Locker, J., Nilsson, T., Goud, B., Söling, H.D., Tang, B.L.,
1114 Wong, S.H., and Hong, W. (1994). Localization of the Lys, Asp, Glu, Leu tetrapeptide
1115 receptor to the Golgi complex and the intermediate compartment in mammalian cells. J.
1116 Cell Biol. 127: 1557 LP-1574.
1117 Hadlington, J. and Denecke, J. (2000). Sorting of soluble proteins in the secretory pathway of
1118 plants. Curr. Opin. Plant Biol.: 461–468.
1119 Hsu, V., Shah, N., and Klausner, R. (1992). A brefeldin A-like phenotype is induced by the
1120 overexpression of a human ERD-2-like protein, ELP-1. Cell 69: 625–635.
1121 Ito, Y., Uemura, T., Shoda, K., Fujimoto, M., Ueda, T., and Nakano, a. (2012). cis-Golgi
1122 proteins accumulate near the ER exit sites and act as the scaffold for Golgi regeneration
1123 after brefeldin A treatment in tobacco BY-2 cells. Mol. Biol. Cell 23: 3203–3214.
1124 Klinger, C.M., Ramirez-Macias, I., Herman, E.K., Turkewitz, A.P., Field, M.C., and Dacks, J.B.
1125 (2016). Resolving the homology—function relationship through comparative genomics of
1126 membrane-trafficking machinery and parasite cell biology. Mol. Biochem. Parasitol.
1127 Koch, G.L. (1987). Reticuloplasmins: a novel group of proteins in the endoplasmic reticulum. J.
1128 Cell Sci. 87 (Pt 4): 491–492.
1129 Lee, H.-I., Gal, S., Newman, T.C., and Raikhel, N. V (1993). The Arabidopsis Endoplasmic
1130 Reticulum Retention Receptor Functions in Yeast. Source Proc. Natl. Acad. Sci. United

States Am. Plant Biol. 90: 11433–11437.

Lewis, M. and Pelham, H. (1990). A human homologue of the yeast HDEL receptor. Nature 348: 162–163.

Lewis, M. and Pelham, H. (1992). Ligand-induced redistribution of a human KDEL receptor from the Golgi complex to the endoplasmic reticulum. Cell 66: 353–364.

Lewis, M., Sweet, D., and Pelham, H. (1990). The ERD2 gene determines the specificity of the luminal ER protein retention system. Cell 61: 1359–1363.

Li, J., Zhao-Hui, C., Batoux, M., Nekrasov, V., Roux, M., Chinchilla, D., Zipfel, C., and Jones, J.D.G. (2009). Specific ER quality control components required for biogenesis of the plant innate immune receptor EFR. Proc. Natl. Acad. Sci. 106: 15973–15978.

Macer, D.R. and Koch, G.L. (1988). Identification of a set of calcium-binding proteins in reticuloplasm, the luminal content of the endoplasmic reticulum. J. Cell Sci. 91 (Pt 1): 61–70.

Majoul, I., Straub, M., Hell, S.W., Duden, R., and Söling, H.D. (2001). KDEL-Cargo Regulates Interactions between Proteins Involved in COPI Vesicle Traffic: Measurements in Living Cells Using FRET. Dev. Cell 1: 139–153.

MALIGA, P., SZ.-BREZNOVITS, Á., and MÁRTON, L. (1973). Streptomycin-resistant Plants from Callus Culture of Haploid Tobacco. Nat. New Biol. 244: 29–30.

Martínez-Alonso, E., Tomás, M., and Martínez-Menárguez, J.A. (2013). Golgi tubules: their structure, formation and role in intra-Golgi transport. Histochem. Cell Biol. 140: 327–339.

Mei, M., Zhai, C., Li, X., Zhou, Y., Peng, W., Ma, L., Wang, Q., Iverson, B.L., Zhang, G., and Yi, L. (2017). Characterization of aromatic residue–controlled protein retention in the endoplasmic reticulum of Saccharomyces cerevisiae. J. Biol. Chem. 292: 20707–20719.

Montesinos, J.C., Pastor-Cantizano, N., Robinson, D.G., Marcote, M.J., and Aniento, F. (2014). Arabidopsis p24δ5 and p24δ9 facilitate Coat Protein I-dependent transport of the K/HDEL receptor ERD2 from the Golgi to the endoplasmic reticulum. Plant J. 80: 1014–1030.

Munro, S. and Pelham, H. (1987). A C-terminal signal prevents secretion of luminal ER proteins. Cell 48: 899–907.

Murashige, T. and Skoog, F. (1962). A Revised Medium for Rapid Growth and Bio Assays with Tobacco Tissue Cultures. Physiol. Plant. 15: 473–497.

Palade, G. (1975). Intracellular aspects of the process of protein synthesis. Science 189: 867.

1163 Pelham, H.R.B. (1988). Evidence that luminal ER proteins are sorted from secreted proteins in
1164 a post-ER compartment. EMBO J. 7: 913–918.
1165 Pfeffer, S.R. (2007). Unsolved mysteries in membrane traffic. Annu. Rev. Biochem. 76: 629–
1166 645.
1167 Phillipson, B. a, Pimpl, P., daSilva, L.L., Crofts, a J., Taylor, J.P., Movafeghi, a, Robinson,
1168 D.G., and Denecke, J. (2001). Secretory bulk flow of soluble proteins is efficient and
1169 COPII dependent. Plant Cell 13: 2005–2020.
1170 Pimpl, P., Taylor, J.P., Snowden, C., Hillmer, S., Robinson, D.G., and Denecke, J. (2006).
1171 Golgi-mediated vacuolar sorting of the endoplasmic reticulum chaperone BiP may play an
1172 active role in quality control within the secretory pathway. Plant Cell 18: 198–211.
1173 Pulvirenti, T. et al. (2008). A traffic-activated Golgi-based signalling circuit coordinates the
1174 secretory pathway. Nat. Cell Biol. 10: 912–922.
1175 Rose, J.K. and Doms, R.W. (1988). Regulation of Protein Export From the Endoplasmic
1176 Reticulum. Annu. Rev. Cell Biol. 4: 257–288.
1177 Scheel, A. a and Pelham, H.R.B. (1998). Identification of Amino Acids in the Binding Pocket of
1178 the Human KDEL Receptor. J. Biol. Chem. 273: 2467–2472.
1179 Schmid, M., Davison, T.S., Henz, S.R., Pape, U.J., Demar, M., Vingron, M., Schölkopf, B.,
1180 Weigel, D., and Lohmann, J.U. (2005). A gene expression map of Arabidopsis thaliana
1181 development. Nat. Genet. 37: 501–506.
1182 Semenza, J., Hardwick, K., Dean, N., and Pelham, H. (1990). ERD2, a yeast gene required for
1183 the receptor-mediated retrieval of luminal ER proteins from the secretory pathway. Cell 61:
1184 1349–1357.
1185 Singh, P., Tang, B.L., Wong, S.H., and Hong, W. (1993). Transmembrane Topology of the
1186 Mammalian KDEL Receptor. Mol. Cell. Biol. 13: 6435–6441.
1187 Snapp, E. (2005). Design and Use of Fluorescent Fusion Proteins in Cell Biology. Curr. Protoc.
1188 Cell Biol. 27: 21.4.1-21.4.13.
1189 Sönnichsen, B., Füllekrug, J., Nguyen Van, P., Diekmann, W., Robinson, D.G., and Mieskes,
1190 G. (1994). Retention and retrieval: both mechanisms cooperate to maintain calreticulin in
1191 the endoplasmic reticulum. J. Cell Sci. 107 (Pt 1: 2705–17.
1192 Sparkes, I. a, Runions, J., Kearns, A., and Hawes, C. (2006). Rapid, transient expression of
1193 fluorescent fusion proteins in tobacco plants and generation of stably transformed plants.
1194 Nat. Protoc. 1: 2019–2025.

Spiess, M. (1995). Heads or tails - what determines the orientation of proteins in the membrane. FEBS Lett. 369: 76–79.

Sweet, D.J. and Pelham, H.R. (1992). The Saccharomyces cerevisiae SEC20 gene encodes a membrane glycoprotein which is sorted by the HDEL retrieval system. EMBO J. 11: 423–32.

Tang, B.L., Wong, S.H., Qi, X.L., Low, S.H., and Hong, W. (1993). Molecular cloning, characterization, subcellular localization and dynamics of p23, the mammalian KDEL receptor. J. Cell Biol. 120: 325–38.

Townsley, F.M., Frigerio, G., and Pelham, H.R.B. (1994). Retrieval of HDEL proteins is required for growth of yeast cells. J. Cell Biol. 127: 21–28.

Townsley, F.M., Wilson, D.W., and Pelham, H.R. (1993). Mutational analysis of the human KDEL receptor: distinct structural requirements for Golgi retention, ligand binding and retrograde transport. EMBO J. 12: 2821–2829.

Valls, L., Hunter, C., Rothman, J., and Stevens, T. (1987). Protein sorting in yeast: the localization determinant of yeast vacuolar carboxypeptidase Y resides in the propeptide. Cell 48: 887–897.

vonHeijne, G. (1989). Control of topology and mode of assembly of a polytopic membrane protein by positively charged residues. Nature 341: 456–458.

Wieland, F., Gleason, M., Serafini, T., and Rothman, J. (1987). The rate of bulk flow from the endoplasmic reticulum to the cell surface. Cell 50: 289–300.

Xu, G., Li, S., Xie, K., Zhang, Q., Wang, Y., Tang, Y., Liu, D., Hong, Y., He, C., and Liu, Y. (2012). Plant ERD2-like proteins function as endoplasmic reticulum luminal protein receptors and participate in programmed cell death during innate immunity. Plant J. 72: 57–69.

Xu, G. and Liu, Y. (2012). Plant ERD2s self-interact and interact with GTPase-activating proteins and ADP-ribosylation factor 1. Plant Signal. Behav. 7: 1092–1094.

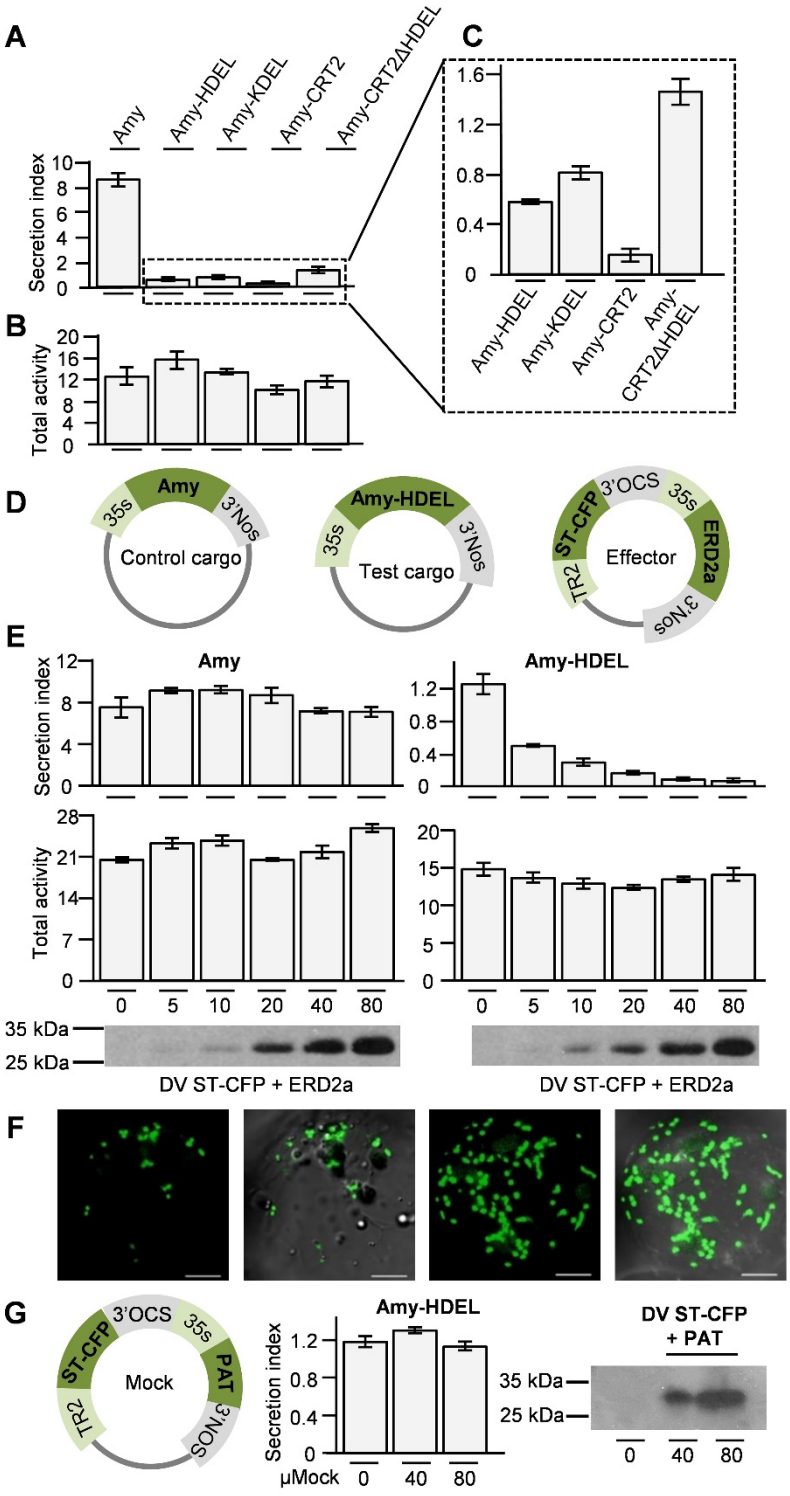

Figure 1. Ligand characterization and quantitative dose-response activity essay for Arabidopsis ERD2a
A) Secreted α-amylase (Amy) and its recombinant fusions, bearing different ER retention signals (Amy-HDEL, Amy-KDEL, Amy-CRT2 and Amy-CRT2ΔHDEL), were transiently expressed in *Nicotiana tabacum* protoplasts for 24 hours. The secretion index of each fusion is the ratio between the activity from the medium divided by the activity in the cells. 50 µg was used of each plasmid DNA preparation. **B)** The total α-amylase activity obtained in each cell suspension given in arbitrary relative units (ΔO.D./ml/min). **C)** Secretion index of cell retained fusions from panel A) for close-up comparison. **D)** Schematic of plasmids used for a quantitative gain-of-function assay, showing single gene expression plasmids for control cargo and test cargo under the transcriptional control of the 35S promoter. The Effector plasmid is a dual gene expression vector (Bottanelli et al., 2012) with a TR2:promoter-driven Golgi-marker ST-CFP and 35S:promoter-driven ERD2a. **E)** Dose-response assay in *Nicotiana benthamiana* protoplasts with a constant amount of either Amy (top left) or Amy-HDEL (top right) plasmids (50 µg in each case) and increasing concentrations of effector plasmid indicated below each lane as µg of DNA. Shown is the secretion index (top panel) and the total activity (bottom panel) in function of effector plasmid dosage, Transfection efficiency of the effector plasmid is visualised by immunoblotting with anti GFP serum showing a 32kDa ST-CFP band. The negative controls contain only cargo DNA. Error bars are standard deviations of three independent protoplast transfections (biological replicates). **F)** Confocal laser scanning of transfected protoplasts using the highest dose of the effector plasmid in dark and light field. The second pair of images show maximum intensity projections. Scale bars are 10 µm. **G)** Control experiment to show that the internal marker ST-CFP does not influence amy-HDEL transport.

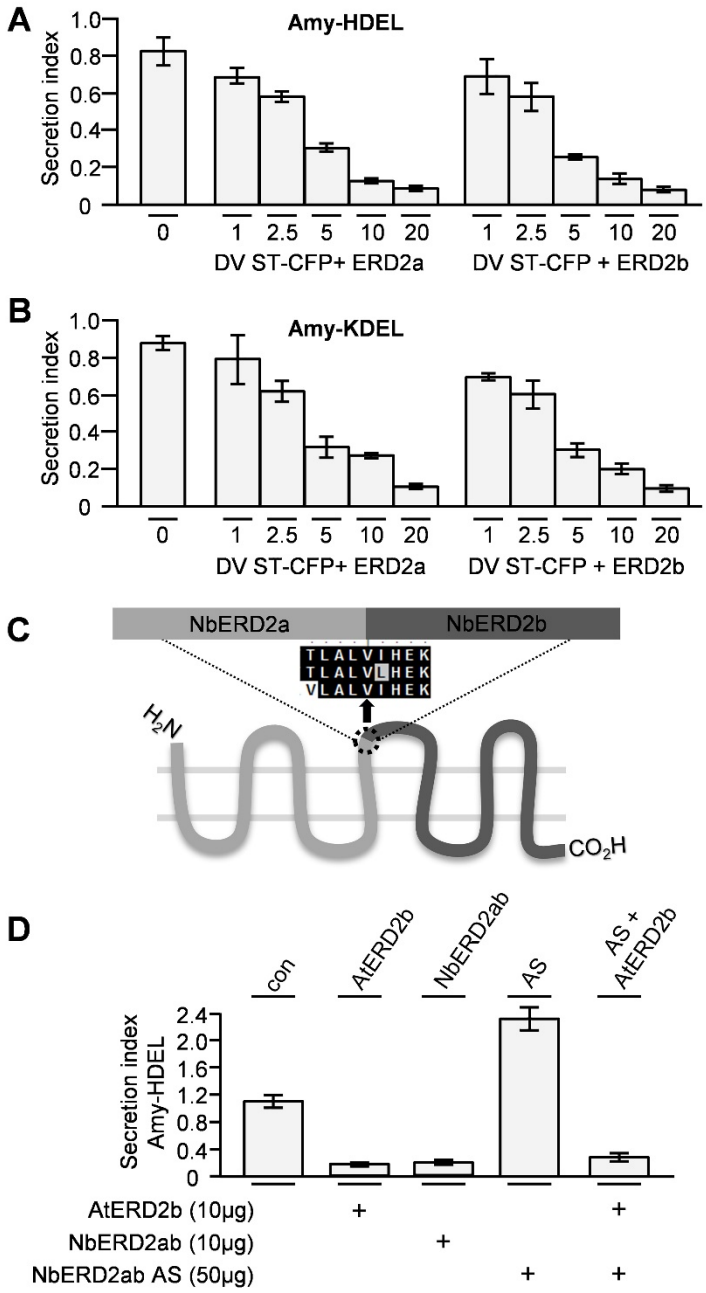

Figure 2. Evaluation of signal specificity and evolutionary conservation of *ERD2* genes in *Arabidopsis thaliana* and *Nicotiana benthamiana*.

A) Dose-response assays and experimental setup as in Figure 1E, but comparing ERD2a with ERD2b on amy-HDEL and using lower amounts of effector plasmids (indicated below each lane in µg). Notice the lack of any difference between ERD2a or ERD2b. **B)** Identical experiment as panel A, but with amy-KDEL as cargo instead of Amy-HDEL. **C)** Illustration of the hybrid *ERD2* transcript (*NbERD2ab*) which was generated as sense and as anti-sense constructs. The alignment shows the point where the fusion was made to generate a hybrid *ERD2* coding region. **D)** Transient expression experiment with *Nicotiana benthamiana* protoplasts co-expressing Amy-HDEL with either *AtERD2b*, sense *NbERD2ab*, antisense *NbERD2ab* (AS) or the combination of AS with *AtERD2b* and incubated for 48 hours to allow degradation of endogenous ERD2. 50 µg of cargo plasmid was electroporated alone or co-electroporated together with sense or antisense *ERD2* plasmids as indicated by "+". Error bars are standard deviations of three independent transfections.

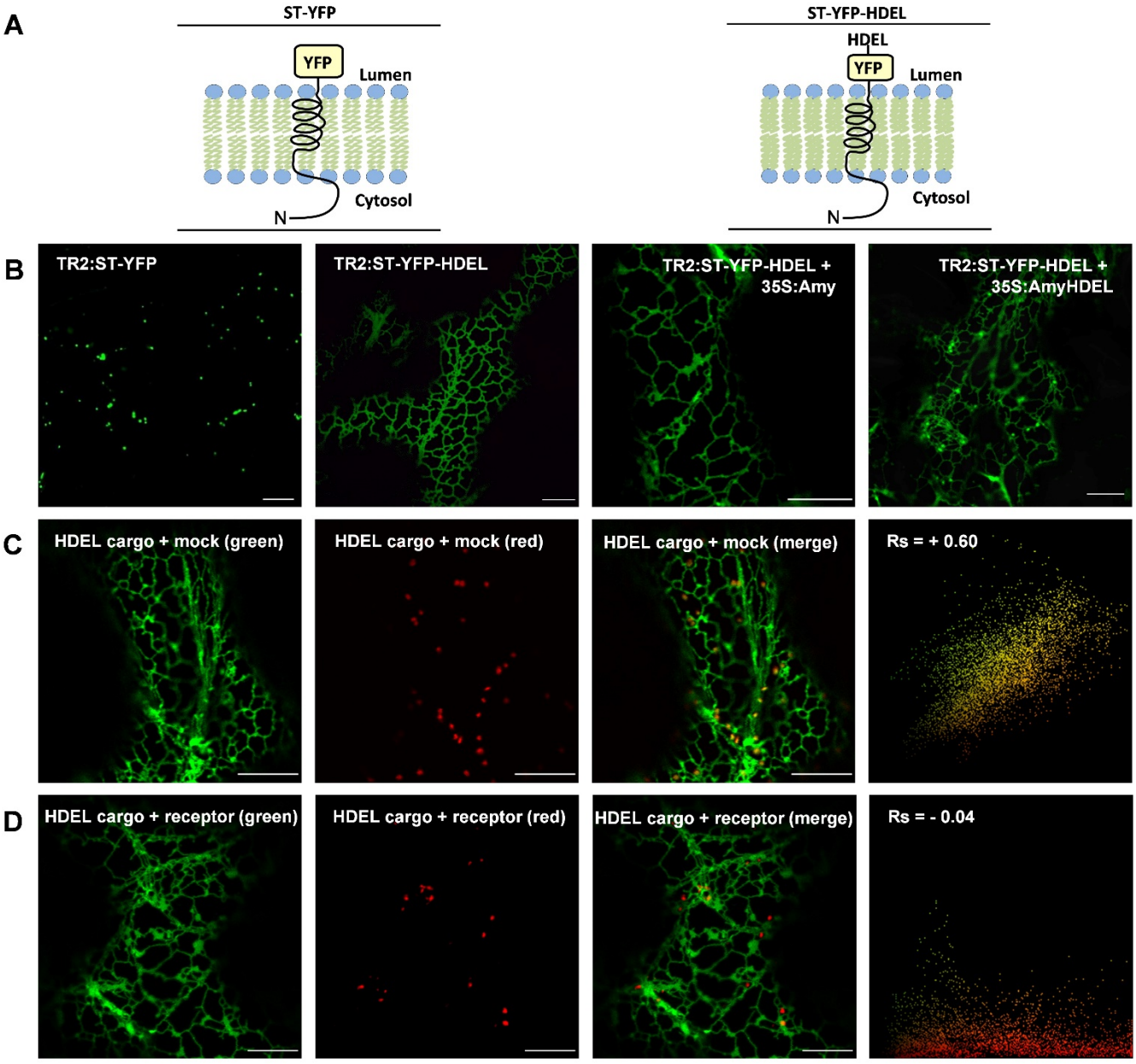

Figure 3. ERD2 mediated ER retention *in situ*

A) Illustration of the membrane topology of the Golgi-marker ST-YFP and ST-YFP-HDEL with the amino-terminus (N) in the cytosol and the YFP exposed in the lumen. **B)** Confocal laser scanning microscopy (CLSM) images from infiltrated tobacco leaves showing the sub-cellular localisation of ST-YFP and its variant ST-YFP-HDEL under control of the weak *TR2* promoter alone (left two panels). The two panels to the right show ST-YFP-HDEL expression in the presence of the strong CaMV35S promoter-mediated over-expression of either Amy or Amy-HDEL from the same T-DNA. **C)** The dual HDEL cargo expression vector (TR2:ST-YFP-HDEL + 35S:Amy-HDEL) was co-infiltrated with a second dual expression vector encoding the Golgi marker TR2:ST-RFP together with a neutral effector 35S:PAT for control purposes (mock). Notice that punctate ST-YFP-HDEL structures colocalise with the Golgi signals confirming their identity (white arrow heads). The scatterplot from multiple images analysed for punctate structures only shows a single yellow population and a positive Spearman correlation coefficient (Rs). **D)** Suppression of saturation: The same experiment as in panel C, but the neutral effector 35S:PAT was replaced by 35S:ERD2 (receptor). Notice the lack of ST-YFP-HDEL signals in the red Golgi bodies. White arrowheads show red fluorescence in red and merged channels, but no fluorescence in the green channel. The scatterplot from multiple images analysed for punctate structures only shows a predominantly red pixel population. Occasional overlap with green fluorescence is due to vicinity to the ER but does not correlate, as indicated by a negative Rs value. Scale bars in all panels are 10 µm. See Supplemental Figure 1A,B for alternative colour combinations.

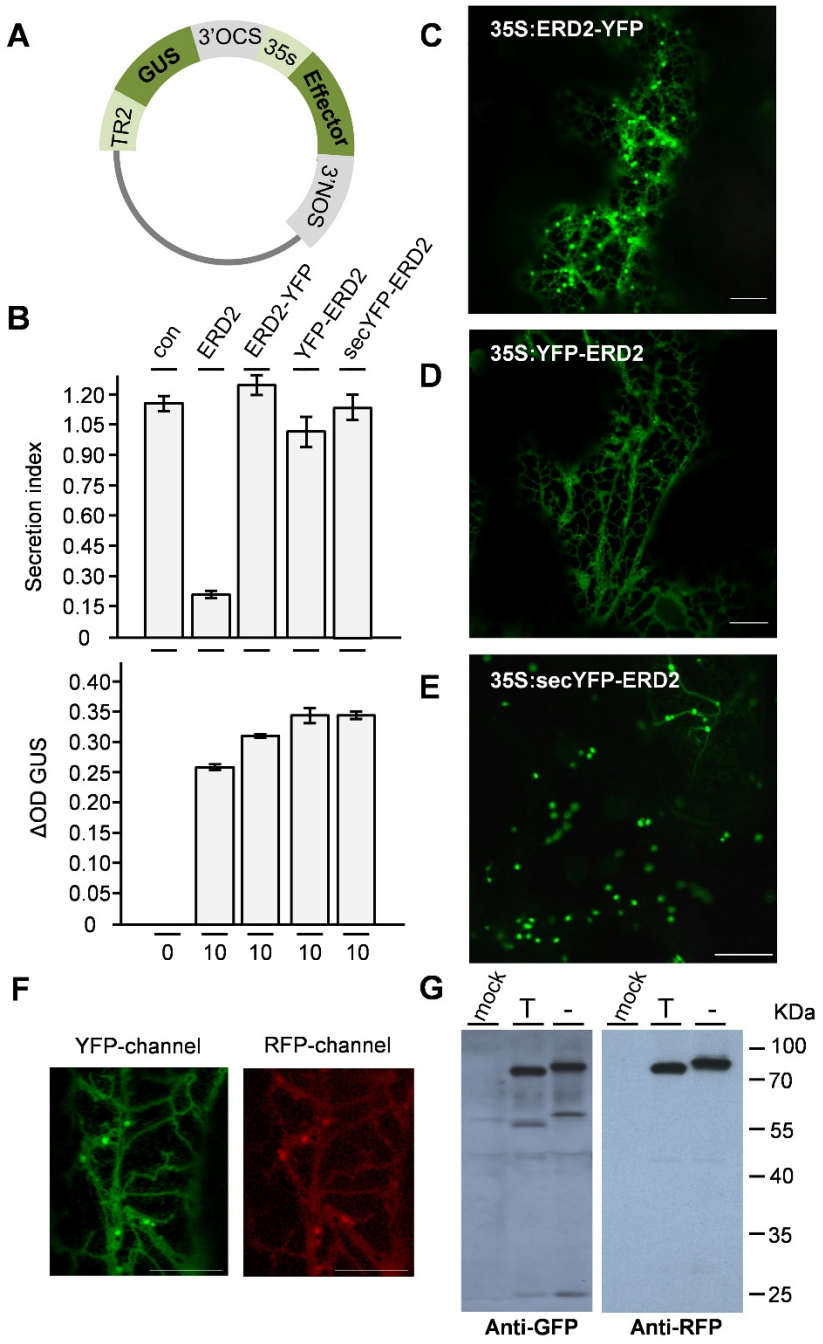

Figure 4. Comparison of three different fluorescent ERD2 fusions

A) Schematic of dual expression system used for the assay based on the pGUSref plasmid (Gershlick et al., 2014) allowing normalisation of the transfection efficiency by the colorimetric GUS assay. **B)** Transient expression experiment with *Nicotiana benthamiana* protoplasts co-expressing Amy-HDEL with either wild type ERD2 or three different fluorescent fusions to YFP (ERD2-YFP, YFP-ERD2 or secYFP-ERD2). 50 µg of cargo plasmid was electroporated together with effector plasmid amounts indicated below each lane. Error bars are standard deviation of three independent transfections. The upper panel shows the amy-HDEL secretion index whilst the bottom panel shows the internal marker GUS (arbitrary relative units). **C)** CLSM images of tobacco leaf epidermis cells expressing 35S promoter-driven ERD2-YFP, showing ER and punctate fluorescence. **D)** As in C, but YFP-ERD2 showing ER-only pattern. **E)** secYFP-ERD2 showing punctate-only pattern. Scale bar: 10 µm. Notice that three different fusions show three different subcellular localisation patterns (compare C, D and E), none of which show biological activity in the bio-assay. **F)** Control experiment to show that C-terminally fused RFP causes partial ER retention of secYFP-ERD2-RFP. All scale bars are 10µm and promoters used are indicated in each panel. **G)** Transient expression of fusion protein secYFP-ERD2-RFP in tobacco protoplasts in the presence (T) or the absence (-) of Tunicamycin. Immunoblots were probed with anti-GFP (left) or anti-RFP (right) serum. Mock refers to the negative control and consists of an extract prepared from protoplasts electroporated without plasmids. The positions of the size markers are indicated on the right and given in kiloDaltons (kDa). Notice the distinct size-shift of the full-length fusion protein.

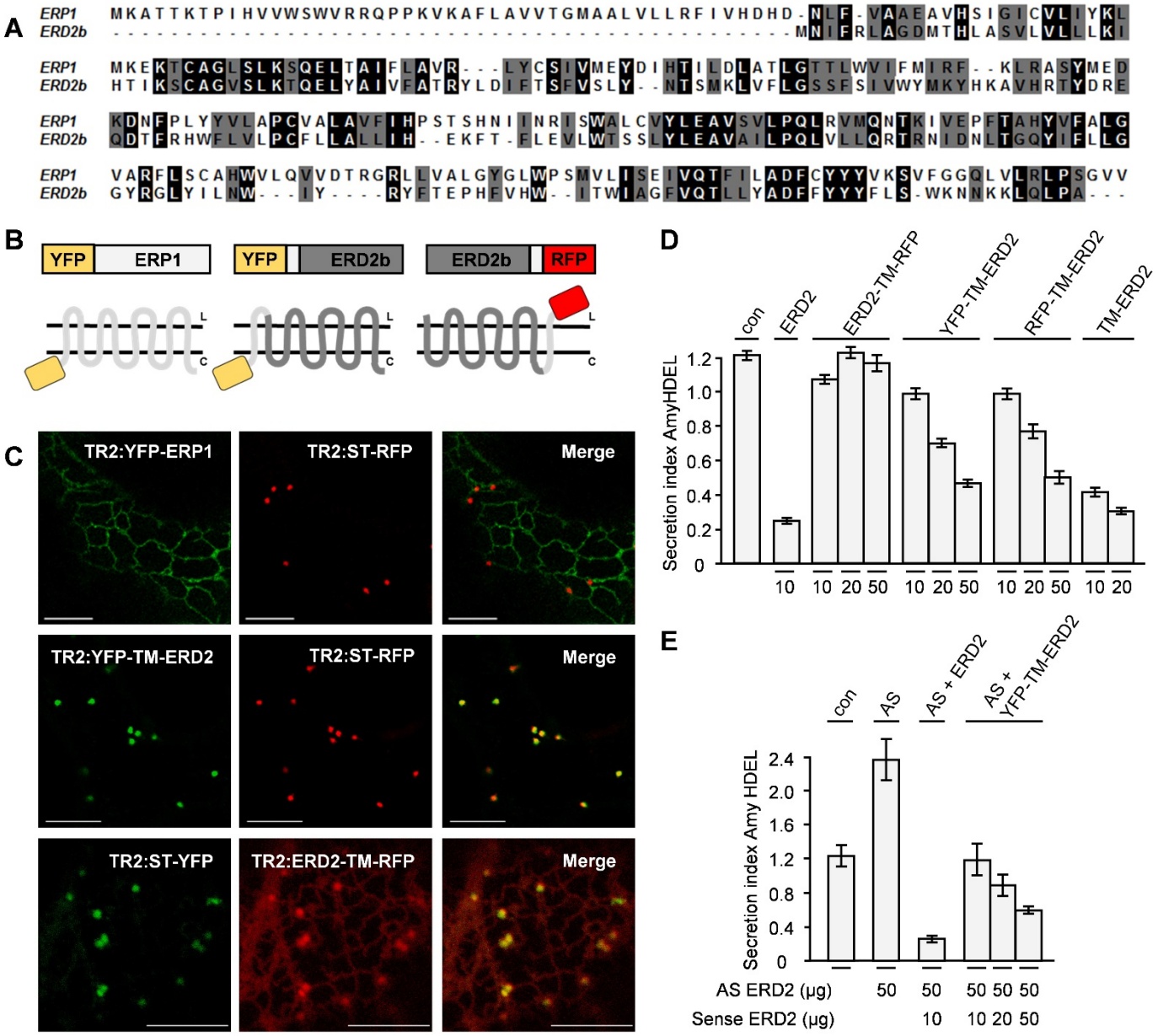

Figure 5. Addition of a transmembrane domain to either the C-terminus or the N-terminus of ERD2

A) Alignment of AtERP1 with AtERD2b. **B)** Illustration of chimeric constructs. **C)** Confocal laser scanning microscopy in leaf epidermis cells comparing the subcellular distribution of YFP-ERP1 and the hybrid YFP-TM-ERD2 with the Golgi-marker ST-RFP (upper two panels). The bottom panel shows the subcellular distribution of the hybrid ERD2-TM-RFP compared to the Golgi marker ST-YFP. All constructs are driven by the TR2 promoter. **D)** Co-expression of the Amy-HDEL with ERD2 and fusions containing an additional transmembrane domain at the N-terminus (YFP-TM-ERD2, RFP-TM-ERD2 and TM-ERD2) or the C-terminus (ERD2-TM-RFP) in *Nicotiana benthamiana* protoplasts. 50 µg of amy-HDEL was co-transfected with amounts of effector plasmids given below each lane in µg. All annotations are as in Figure 1. Notice that only the N-terminal fusions with an additional transmembrane domain retain biological activity. **E)** Knocking-down the endogenous *ERD2* using the antisense (AS) *NbERD2ab* and complementation of the activity either by the sense wild-type *ERD2* (*AtERD2b*) or by the biologically active fusion YFP-TM-ERD2. Experimental conditions are as in Figure 2D.

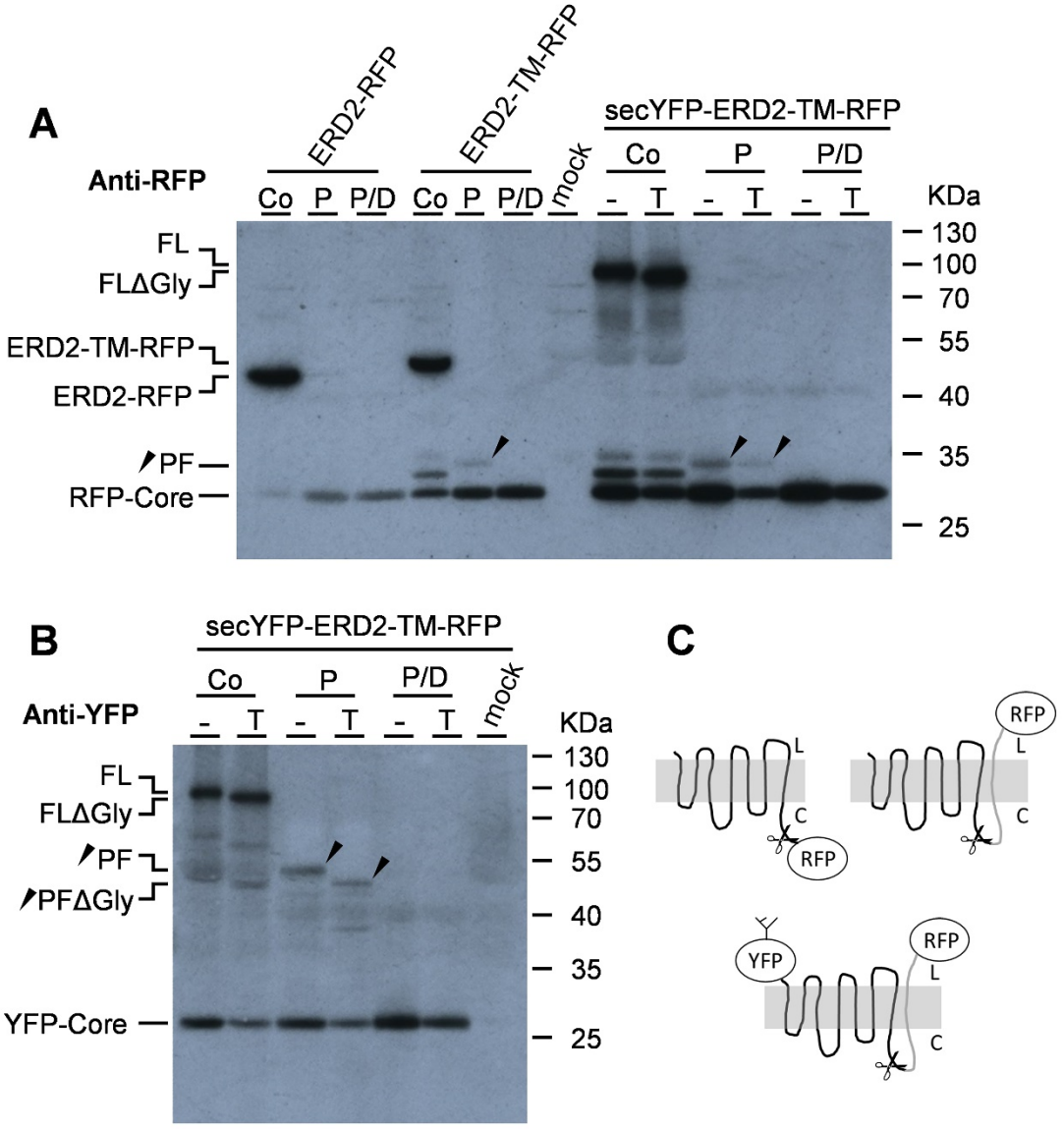

Figure 6. Experiments using modifications of the ERD2 C-terminus
A) Protease protection analysis of transiently expressed fusion proteins ERD2-RFP, ERD2-TM-RFP, and secYFP-ERD2-TM-RFP in tobacco protoplasts with (T) or without (-) Tunicamycin. Osmotically stabilised cell extracts containing intact microsomes were either untreated (Co) or digested with Proteinase K alone (P) or digested together with detergent (P/D). Immunoblots were probed with anti-RFP serum and included a control lane with an extract from mock-transfected cells as negative control (mock). Individual polypeptide bands include the full length fusion proteins ERD2-TM-RFP and ERD2-RFP, secYFP-ERD2-TM-RFP with (FL) and without glycan (FLΔGly), the specific protease protected fragment (PF) and the RFP-core. The positions of the size markers are indicated on the right and given in kiloDaltons. The black arrowhead indicates the position of the PF in the relevant lanes. **B)** Protease protection analysis as in A) but secYFP-ERD2-TM-RFP lanes probed with anti GFP serum. Abbreviations are as in B). **C)** Schematic drawing of the protein fusions ERD2-RFP, ERD2-TM-RFP, and secYFP-ERD2-TM-RFP with their proposed membrane topologies and the site where proteinase K is likely to cleave the fusion protein (scissors). Notice that all further predicted cytosolic loops of ERD2 appear to be resistant to the protease.

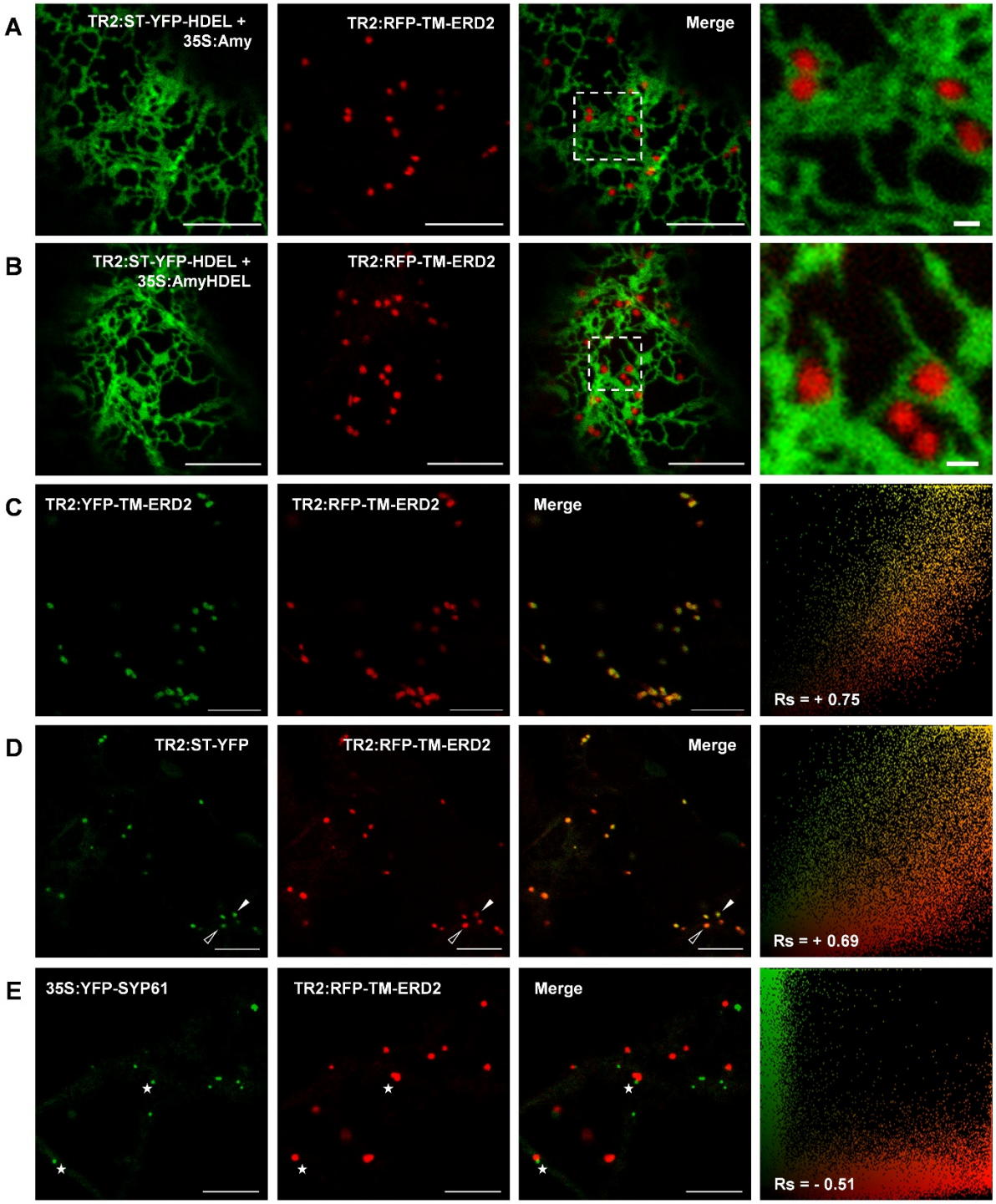

Figure 7. Testing the co-localization of biologically active ERD2 fusions
A) CLSM showing the distribution of RFP-TM-ERD2 in the absence of ligand over-expression by co-expression with the control construct (TR2:ST-YFP-HDEL + 35S:Amy). **B)** CLSM demonstrating *in situ* biological function of RFP-TM-EDR2 co-expressed with the HDEL overdose test construct (TR2:ST-YFP-HDEL + 35S:AmyHDEL). Scale bars are 10 µm. Close-ups of the enlarged dashed rectangle in C) and D) show that RFP-TM-ERD2 punctae are well separated from the ER. Scale bars in the close-ups are 1 µm. See Supplemental Figure 4A for alternative colour combinations and Figure 4B for correlation analysis. **C)** CLSM image showing YFP-TM-ERD2 co-expressed with RFP-TM-ERD2 showing high level of co-localisation, illustrated by a single yellow pixel population in the scatterplot and a high positive Rs. **D)** CLSM image of RFP-TM-ERD2 co-expressed with the Golgi-marker ST-YFP showing consistent co-labelling of the same Golgi bodies, but with less correlation between green and red signals, showing a range between mostly red (open arrowheads) or mostly green (white arrowheads) structures, reflected by a broader scatterplot and a lower Rs. **E)** CLSM image of RFP-TM-ERD2 co-expressed with the TGN–marker YFP-SYP61, showing totally separate structures that are either green or red. A strong negative Rs and two completely separate pixel populations demonstrate a complete lack of co-localisation even when found adjacent to each other (white stars). All scale bars are 10 µm.

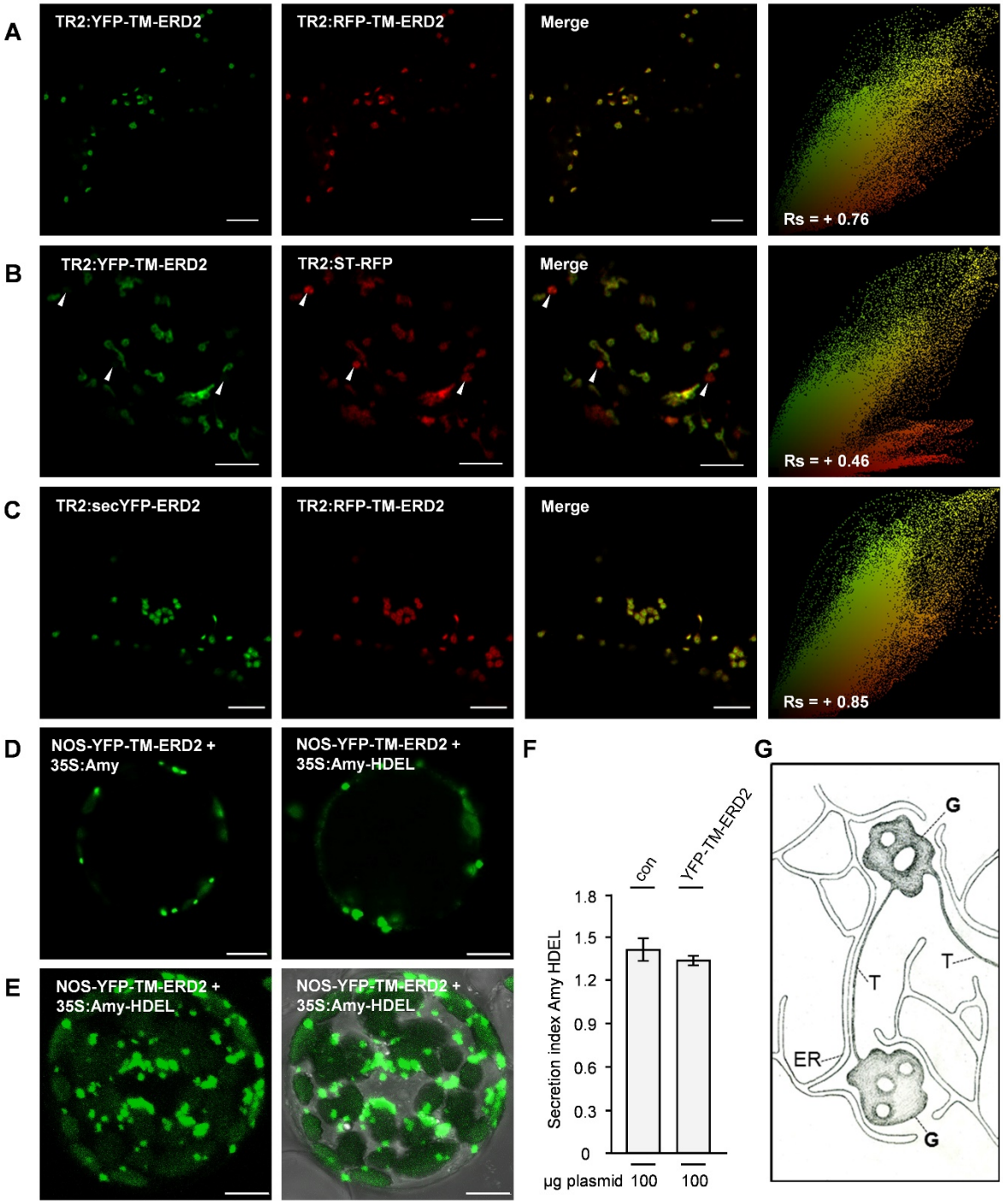

Figure 8. Evidence that ERD2 localisation is restricted to early Golgi cisternae even when ligands are overexpressed.

A) CLSM using higher resolution Airyscan detector showing strong co-localisation of YFP-TM-ERD2 and RFP-TM-ERD2. Scatterplot and Spearman correlation coefficient were similar to data from conventional CLSM (Figure 7), confirming that both fusions can substitute for each other. **B)** CLSM using higher resolution Airy scan detector showing YFP-TM-ERD2 co-expressed with the Golgi-marker ST-RFP shows a clear segregation of structures labelled solely by ST-RFP (white arrow heads) as revealed by the distinct red population on the scatter plot and a significantly lower correlation coefficient**. C)** CLSM using higher resolution Airy scan detector of non-functional secYFP-ERD2 and functional RFP-TM-ERD2, revealing a very strong co-localisation. Scale bars on panels A), B) and C) are 5 µm. **D)** Confocal laser scanning microscopy of a typical transfected *Nicotiana benthamiana* protoplast with triple expression vector (Supplemental Methods 2) in dark field, showing the ERD2 localisation in the presence of non-ligand (Amy) versus ligand (Amy-HDEL) overexpression. **E)** Maximum intensity projection of a transfected protoplast in E) in dark field (left) and bright field (right), showing no evidence of any green fluorescence in an ER network. Scale bars are 10 µm. **F)** Secretion index of the protoplast suspensions corresponding to D,E, showing the expression of Amy-HDEL alone (con) or with YFP-TM-ERD2. **G)** Schematic drawing of early Golgi cisternae (G) connected by thin tubules (T), surrounded by an ER network (ER).

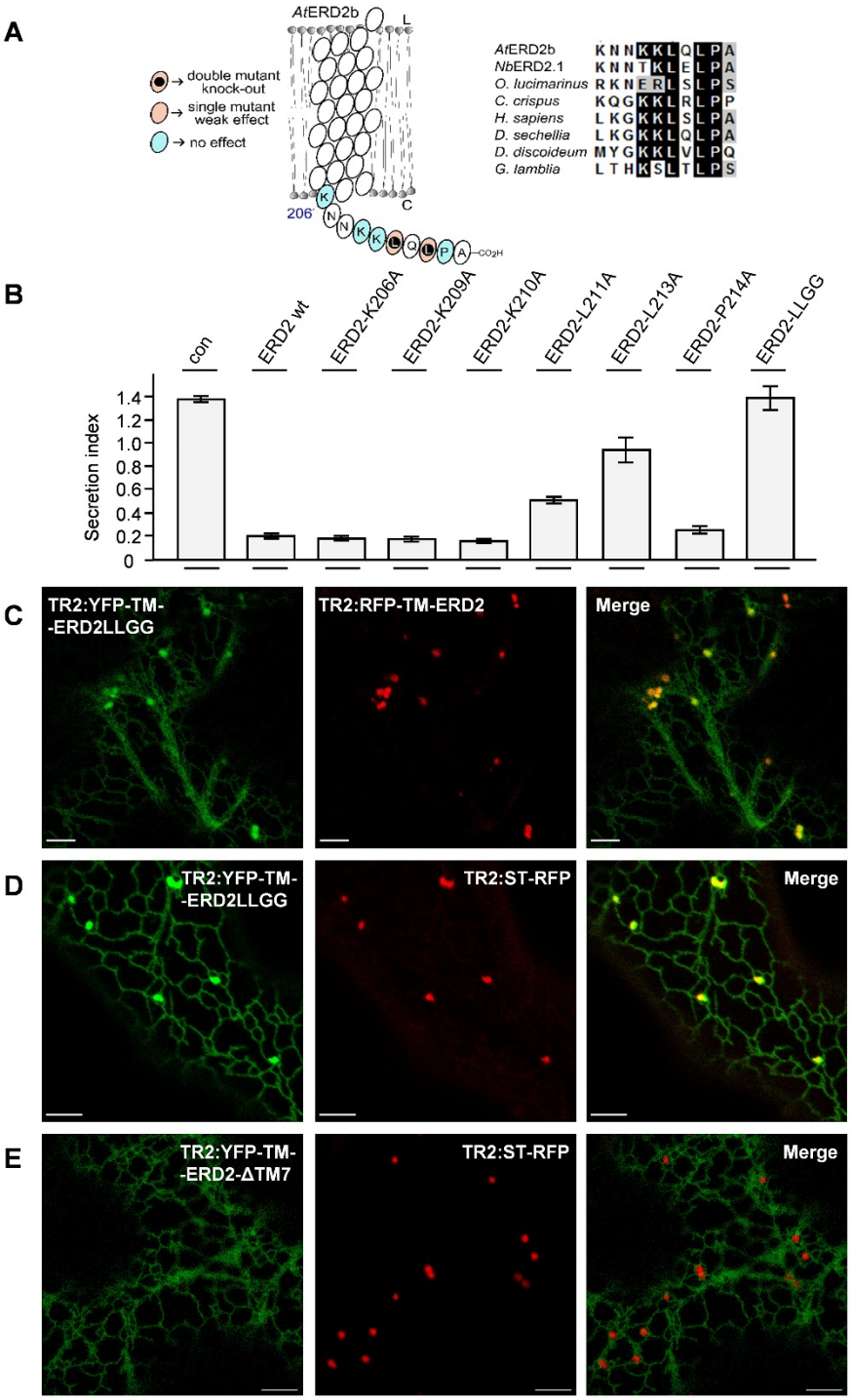

Figure 9. The C-terminus of ERD2 controls efficient ER export and is essential for its biological activity.
A) Illustration of point mutagenesis of the C-terminus and the observed effects in the biological activity followed by an alignment of ERD2 C-termini from different eukaryotes as indicated. **B)** Co-expression of the Amy-HDEL with wild-type ERD2 (wt) and individual Alanine-replacement mutants in the cytosolic tail of ERD2 in *Nicotiana benthamiana* protoplasts. 50 µg of amy-HDEL plasmid was co-transfected with 10 µg of effector plasmids. All annotations are as in Figure 1. Mutants that compromise biological activity are identified by increased secretion indices compared to the wild type ERD2. The double mutant (LLGG) has both conserved leucines (L211 and L213) replaced by the smaller amino acid glycine. **C)** CLSM showing the distribution of YFP-TM-ERD2-LLGG in comparison with RFP-TM-ERD2. Scale bars are 5 µm. **D)** YFP-TM-ERD2-LLGG in comparison with the Golgi marker ST-RFP. Scale bars are 5 µm. Notice that the non-functional LLGG mutant still reached the Golgi apparatus but was now markedly retained in the ER, similar to the C-terminal fusion ERD2-YFP (see Figure 4C). **E)** Deletion of the last TM domain and cytosolic tail (YFP-TM-ERD2-ΔTM7) caused complete ER retention. Experimental conditions/annotations as in D.

Predominant Golgi-residency of the plant K/HDEL receptor is essential for its function in mediating ER retention

Fernanda Aparecida Lima Silva-Alvim, Jing An, Jonas Chaves Alvim, Ombretta Foresti, Alexandra Grippa, Alexandra J.E. Pelgrom, Thomas Lewis Adams, Chris Hawes and Jurgen Denecke

Plant Cell; originally published online August 2, 2018;
DOI 10.1105/tpc.18.00426